DECLARATION OF JUNE ANN MUNFORD

1. My name is June Ann Munford. I am over the age of 18, have personal knowledge of the facts set forth herein, and am competent to testify to the same.

2. I earned a Master of Library and Information Science (MLIS) from the University of Wisconsin-Milwaukee in 2009. I have over ten years of experience in the library/information science field. Beginning in 2004, I have served in various positions in the public library sector including Assistant Librarian, Youth Services Librarian and Library Director. I have attached my Curriculum Vitae as Appendix CV.

3. During my career in the library profession, I have been responsible for materials acquisition for multiple libraries. In that position, I have cataloged, purchased and processed incoming library works. That includes purchasing materials directly from vendors, recording publishing data from the material in question, creating detailed material records for library catalogs and physically preparing that material for circulation. In addition to my experience in acquisitions, I was also responsible for analyzing large collections of library materials, tailoring library records for optimal catalog

search performance and creating lending agreements between libraries during my time as a Library Director.

4. I am fully familiar with the catalog record creation process in the library sector. In preparing a material for public availability, a library catalog record describing that material would be created. These records are typically written in Machine Readable Catalog (herein referred to as "MARC") code and contain information such as a physical description of the material, metadata from the material's publisher, and date of library acquisition. In particular, the 008 field of the MARC record is reserved for denoting the date of creation of the library record itself. As this typically occurs during the process of preparing materials for public access, it is my experience that an item's MARC record indicates the date of an item's public availability.

5. Typically, in creating a MARC record, a librarian would gather various bits of metadata such as book title, publisher and subject headings among others and assign each value to a relevant numerical field. For example, a book's physical description is tracked in field 300 while title/attribution is tracked in field 245. The 008 field of the MARC record is reserved for denoting the creation of the library record itself. As this is the only date reflecting the inclusion of said materials within the library's collection, it is my experience

that an item's 008 field accurately indicates the date of an item's public availability.

6. I have reviewed Exhibit LGES-1005, "Multi-walled carbon nanotubes functionalized by carboxylic groups: Activation of TiO 2 (anatase) and phosphate olivines (LiMnPO4; LiFePO4) for electrochemical Li-storage" by Ladislav Kavan, et. al as published in *Journal of Power Sources*, August 2010.

7. Attached hereto as Appendix KAVAN01 is a true and correct copy of the MARC record for *Journal of Power Sources* as held by the Penn State University library. I secured this record myself from the library's public catalog. The MARC record contained within Appendix KAVAN01 accurately describes the title, author, publisher, and ISSN number of *Journal of Power Sources.* The 'Publication Frequency' field of this record visible on page 2 indicates this collection includes the August 2010 edition of *Journal of Power Sources* containing "Multi-walled carbon nanotubes functionalized by carboxylic groups: Activation of TiO 2 (anatase) and phosphate olivines (LiMnPO4; LiFePO4) for electrochemical Li-storage".

8. Attached hereto as Appendix KAVAN02 is a true and correct copy of "Multi-walled carbon nanotubes functionalized by carboxylic groups: Activation of TiO 2 (anatase) and phosphate olivines (LiMnPO4; LiFePO4) for electrochemical Li-storage" as published in *Journal of Power Sources* as held by the Penn State University library. I secured this file myself from the library's collection. In comparing Exhibit LGES-1005 to Appendix KAVAN02, it is my determination that Exhibit LGES-1005 is a true and correct copy of "Multi-walled carbon nanotubes functionalized by carboxylic groups: Activation of TiO 2 (anatase) and phosphate olivines (LiMnPO4; LiFePO4) for electrochemical Li-storage" by Ladislav Kavan, et. al as published in *Journal of Power Sources* August 2010.

9. The 008 field of the MARC record in Appendix KAVAN01 indicates the date of record creation. The 008 field of Appendix KAVAN01 indicates the Penn State University library first acquired this journal as of May 27, 1998 and still holds the journal in perpetuity. Considering this information, it is my determination that *Journal of Power Sources* August 2010 and therefore "Multi-walled carbon nanotubes functionalized by carboxylic groups: Activation of TiO 2 (anatase) and phosphate olivines (LiMnPO4; LiFePO4) for electrochemical Li-storage" was made available to the public by Penn State University shortly after its initial release in August 2010.

10. Attached hereto as Appendix KAVAN03 is a true and correct copy of a web page entitled "Multi-walled carbon nanotubes functionalized by carboxylic groups: Activation of TiO 2 (anatase) and phosphate olivines (LiMnPO4; LiFePO4) for electrochemical Li-storage" hosted on the ScienceDirect website at https://www.sciencedirect.com/science/article/abs/pii/S0378775310004180. I secured these screen captures myself.

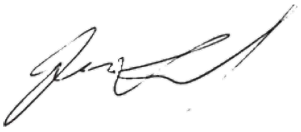
11. Appendix KAVAN03 is a page describing "Multi-walled carbon nanotubes functionalized by carboxylic groups: Activation of TiO 2 (anatase) and phosphate olivines (LiMnPO4; LiFePO4) for electrochemical Li-storage" and contains a link to purchase a full-text copy of this paper. Page 1 of Appendix KAVAN03 indicates "Multi-walled carbon nanotubes functionalized by carboxylic groups: Activation of TiO 2 (anatase) and phosphate olivines (LiMnPO4; LiFePO4) for electrochemical Li-storage" was first made available online via ScienceDirect as of March 12, 2010.

12. I have been retained on behalf of the Petitioner to provide assistance in the above-illustrated matter in establishing the authenticity and public availability of the documents discussed in this declaration. I am being

compensated for my services in this matter at the rate of $200.00 per hour plus reasonable expenses. My statements are objective, and my compensation does not depend on the outcome of this matter.

13. I declare under penalty of perjury that the foregoing is true and correct. I hereby declare that all statements made herein of my own knowledge are true and that all statements made on information and belief are believed to be true; and further that these statements were made the knowledge that willful false statements and the like so made are punishable by fine or imprisonment, or both, under Section 1001 of Title 18 of the United States Code.

Dated: 6/6/2024



June Ann Munford

APPENDIX CV

June A. Munford
Curriculum Vitae

Education

University of Wisconsin-Milwaukee - MS, Library & Information Science, 2009
Milwaukee, WI

- Coursework included cataloging, metadata, data analysis, library systems, management strategies and collection development.
- Specialized in library advocacy, cataloging and public administration.

Grand Valley State University - BA, English Language & Literature, 2008
Allendale, MI

- Coursework included linguistics, documentation and literary analysis.
- Minor in political science with a focus in local-level economics and government.

Professional Experience

Researcher / Expert Witness, October 2017 – present
Freelance ● Pittsburgh, Pennsylvania & Grand Rapids, Michigan

- Material authentication and public accessibility determination. Declarations of authenticity and/or public accessibility provided upon research completion. Experienced with appeals and deposition process.

- Research provided on topics of public library operations, material publication history, digital database services and legacy web resources.

- Past clients include Alston & Bird, Arnold & Porter, Baker Botts, Fish & Richardson, Erise IP, Irell & Manella, O'Melveny & Myers, Perkins-Coie, Pillsbury Winthrop Shaw Pittman and Slayden Grubert Beard.

Library Director, February 2013 - March 2015
Dowagiac District Library ● Dowagiac, Michigan

- Executive administrator of the Dowagiac District Library. Located in

Southwest Michigan, this library has a service area of 13,000, an annual operating budget of over $400,000 and total assets of approximately $1,300,000.

● Developed careful budgeting guidelines to produce a 15% surplus during the 2013-2014 & 2014-2015 fiscal years while being audited.

● Using this budget surplus, oversaw significant library investments including the purchase of property for a future building site, demolition of existing buildings and building renovation projects on the current facility.

● Led the organization and digitization of the library's archival records.

● Served as the public representative for the library, developing business relationships with local school, museum and tribal government entities.

● Developed an objective-based analysis system for measuring library services - including a full collection analysis of the library's 50,000+ circulating items and their records.

November 2010 - January 2013
Librarian & Branch Manager, Anchorage Public Library ● Anchorage, Alaska

● Headed the 2013 Anchorage Reads community reading campaign including event planning, staging public performances and creating marketing materials for mass distribution.

● Co-led the social media department of the library's marketing team, drafting social media guidelines, creating original content and instituting long-term planning via content calendars.

● Developed business relationships with The Boys & Girls Club, Anchorage School District and the US Army to establish summer reading programs for children.

June 2004 - September 2005, September 2006 - October 2013
Library Assistant, Hart Area Public Library
Hart, MI

● Responsible for verifying imported MARC records and original MARC

cataloging for the local-level collection as well as the Michigan Electronic Library.

● Handled OCLC Worldcat interlibrary loan requests & fulfillment via ongoing communication with lending libraries.

Professional Involvement

Alaska Library Association - Anchorage Chapter
- Treasurer, 2012

Library Of Michigan
- Level VII Certification, 2008
- Level II Certification, 2013

Michigan Library Association Annual Conference 2014
- New Directors Conference Panel Member

Southwest Michigan Library Cooperative
- Represented the Dowagiac District Library, 2013-2015

Professional Development

Library Of Michigan Beginning Workshop, May 2008
Petoskey, MI
- Received training in cataloging, local history, collection management, children's literacy and reference service.

Public Library Association Intensive Library Management Training, October 2011
Nashville, TN
- Attended a five-day workshop focused on strategic planning, staff management, statistical analysis, collections and cataloging theory.

Alaska Library Association Annual Conference 2012 - Fairbanks, February 2012
Fairbanks, AK
- Attended seminars on EBSCO advanced search methods, budgeting, cataloging, database usage and marketing.

Depositions

2019 ● Fish & Richardson

Apple v. Qualcomm (IPR2018-001281, 39521-00421IP, IPR2018-01282 and 39521-00421IP2)

2019 ● Erise IP

Implicit, LLC v. Netscout Systems, Inc (Civil Action No. 2:18-cv-53-JRG)

2019 ● Perkins-Coie

Adobe Inc. v. RAH Color Technologies LLC (Cases IPR2019-00627, IPR2019-00628, IPR2019-00629 and IPR2019-00646)

2020 ● O'Melveny & Myers

Maxell, Ltd. v. Apple Inc. (Case No. 5:19-cv-00036-RWS)

2021 ● Pillsbury Winthrop Shaw Pittman LLP

Intel v. SRC (IPR2020-1449)

2022 ● Perkins-Coie

Realtek v. Future Link (IPR2021-01182)

2023 ● Fish & Richardson

Neuroderm Ltd. v. Abbvie, Inc (Case No. PGR2022-00040)

2023 ● Fish & Richardson

Nearmap US Inc. v. Pictometry International Corp. (IPR2022-00735)

2023 ● Fish & Richardson

Samsung Electronics v. MemoryWeb LLC (Case No. 39843-0136PS1)

2023 ● Pillsbury Winthrop Shaw Whitman LLP

Gravel Rating Systems v. Costco Wholesale Corp. (Civil Action No. 4:21-cv-149-ALM)

Limited Case and Clientele History

Alston & Bird

- Ericsson

  v. Collision Communications (IPR2022-01233)

- Nokia

  v. Neptune Subsea, Xtera (Case No. 1:17-cv-01876)

- Universal Electronics Inc

  v. Roku Inc (IPR2022-00818)

Arnold & Porter

- Ivantis

  v. Glaukos (Case No. 8:18-cv-00620)

- Samsung

  v. Jawbone (Case No. 2:21-cv-00186)

Benesch Friedlander Coplan & Aronoff

- Voyis

  v. Cathx (Case No. 5:21-cv-00077-RWS)

Erise I.P.

- Apple
  - v. Ericsson Inc. (IPR2022-00715)
  - v. Future Link Systems (IPRs 6317804, 6622108, 6807505, and 7917680)
  - v. INVT (Case No. 20-1881)
  - v. Navblazer LLC (IPR2020-01253)
  - v. Qualcomm (IPR2018-001281, 39521-00421IP, IPR2018-01282, 39521-00421IP2)
  - v. Quest Nettech Corp (Case No. 2:19-cv-00118-JRG)
  - v. Telefonaktiebolaget LM Ericsson (IPR2022-00275)
- Fanduel
  - v. CGT (Case No. 19-1393)
- Garmin
  - v. Phillips North America LLC (Case No. 2:19-cv-6301-AB-KS)
- Netscout
  - v. Longhorn HD LLC (Case No. 2:20-cv-00349)
  - v. Implicit, LLC (Civil Action No. 2:18-cv-53-JRG)
- Sony Interactive Entertainment LLC
  - v. Bot M8 LLC (IPR2020-01288)
  - v. Infernal Technology LLC (Case No. 2:19-CV-00248-JRG)
- Unified Patents

v. GE Video Compression (Civil Action No. 2:19-cv-248)

Fish & Richardson

- Apple
  - v. AliveCor (3:21-cv-03958)
  - v. LBS Innovations (Case No. 2:19-cv-00119-JRG-RSP)
  - v. Koss Corporation (IPR2021-00305)
  - v. Masimo (IPR 50095-0012IP1, 50095-0012IP2, 50095-0013IP1, 50095-0013IP2, 50095-0006IP1, 50095-0135IP1)
  - v. Neonode (Case No. 21-cv-08872-EMC)
  - v. Qualcomm (IPR2018-001281, 39521-00421IP, IPR2018-01282, 39521-00421IP2)
- Dell
  - v. Neo Wireless (IPR2022-00616)
- Dish Network
  - v. Entropic Communications, LLC (Case No. 2:2023-CV-01043)
  - v. Realtime Adaptive Streaming (Case No. 1:17-CV-02097-RBJ)
  - v. TQ Delta LLC (Case No. 18-1798)
- Evapco Dry Cooling
  - v. SPG Dry Cooling (IPR2021-00688)
- Genetec
  - v. Sensormatic Electronics (Case No. 1:20-CV-00760)
- Huawei

v. Bell Northern Research LLC (IPR2019-01174)

- Kianxis

  v. Blue Yonder (Case No. 3:20-cv-03636)

- LG Electronics

  v. Bell Northern Research LLC (Case No. 3:18-cv-2864-CAB-BLM)

- Metaswitch

  v. Sonus Networks (IPR2018-01719)

- Microsoft

  v. Throughputer Inc (IPR2022-00757)

- Mom Enterprises

  v. Ddrops Company (Case No. 1:22-cv-00332)

- MLC Intellectual Property

  v. MicronTech (Case No. 3:14-cv-03657-SI)

- Nearmap Inc

  v. EagleView Technologies (IPR2022-01009)

- Neuroderm Ltd.

  v. Abbvie, Inc (Case No. PGR2022-00040)

- Realtek Semiconductor

v. Future Link (IPR2021-01182)

- Quectel
  - v. Koninklijke Philips (Case No. 1:20-cv-01710)

- Samsung
  - v. Aire Technology (IPR2022-00877)
  - v. Bell Northern Research (Case No. 2:19-cv-00286-JRG)
  - v. Communication Technologies Inc (IPR2022-01221)
  - v. Jawbone Innovations (IPR2022-00865)
  - v. MemoryWeb LLC (IPR2022-00885)
  - v. Dodots Licensing Solutions (IPR2023-00701)
  - v. Telefonaktiebolaget LM Ericsson (IPR2021-00615)

- Texas Instruments
  - v. Vantage Micro LLC (IPR2020-01261)

- Xilinx
  - v. Sentient Sensors LCC (Case No. 1:22-cv-00173)

Irell & Manella

- Curium

O'Melveny & Myers

- Apple
  - v. Maxell (Case No. 5:19-cv-00036-RWS)

- Micron Technology Inc.

  v. Besang Inc (IPR2023-00900)

- Samsung

  v. Daedalus Prime LLC (1335 Investigation)

Perkins-Coie

- Heru Industries

  v. The UAB Research Foundation (IPR2022-01148)

- Intel Corporation

  v. BitMICRO (Case No. 5:23-cv-00625)

- Realtek Semiconductor

  v. Future Link (IPR2021-01182)

- Twitter Inc

  v. VOIP-Pal.com (Case No. 3:20-cv-02397-JD)

- TCL Industries

  v. Koninklijke Philips NV (IPR2021-00495, IPR2021-00496 and IPR2021-00497)

Pillsbury Winthrop Shaw Pittman

- Intel

  v. FG SRC LLC (Case No. 6:20-cv-00315)

- Gravel Rating Systems

v. Costco (Case No. 4:21-cv-149)
v. Lowe's Home Centers (Case No. 4:21-cv-150)
v. T-Mobile USA (Case No. 4:21-cv-152)
v. Kohl's Inc. (Case No. 4:21-cv-258)
v. Under Armor (Case No. 4:21-cv-356)

Quinn Emanuel

- Wolfspeed

v. The Trustees of Purdue University (Case No. 1:2021-cv-00840)

Stern, Kessler, Goldstein & Fox

- Preliminary Research

Sheppard, Mullin, Richter & Hampton LLP

- Cadence Design Systems Inc.

v. Semiconductor Design Technologies (Case No. 3:23-cv-01001)

APPENDIX KAVAN01

MARC View

LEADER 01721nas a2200421 a 4500				
001 44133696				
003 SIRSI				
005 20240414090109.0				
006 m o d				
007 cr n				
008 980527c19769999sz sx pss 0 a0eng c				
010			a| 2007233220	
016	7		a| 1491915 1 2| DE-600	
019			a| DO NOT EDIT this 360 MARC RECORD	
022			a| 1873-2755 l| 0378-7753 y| 0378-7753	
035			a| (WaSeSS)ssj0001170	
040			a| OH1 b| eng c| OH1 d| OCL d| OCLCQ d| GUA d| VRC d| U9S d| GUA d| OCLCQ d| OCLCF d| OCLCO d| OCLCQ d| SRU d| OCLCO d| OCLCQ d| UAB d| QGK d| WaSeSS	
042			a| pcc	
050	1	4	a| TJ163.2	
130	0		a| Journal of power sources (Online)	
222		0	a| Journal of power sources b| (Online)	
245	1	0	a| Journal of power sources h| [electronic resource].	
260			a| Lausanne : b| Elsevier Sequoia, c| [1976]-	
310			a| 24 issues a year, b| <2007->	
321			a| Frequency varies, b| 1976-	
362	0		a| Vol. 1, issue 1 (Dec. 1976)-	
500			a| Title from contents screen (ScienceDirect, viewed Mar. 9, 2007).	
515			a| Some issues combined.	
538			a| Mode of access: World Wide Web.	
588			a| Latest issue consulted: Vol. 166, issue 1 (Mar. 30, 2007), viewed Mar. 9, 2007.	
650		0	a| Power resources v| Periodicals.	
650		0	a| Power (Mechanics) v| Periodicals.	
650		0	a| Power resources x| Periodicals.	
655		0	a| Electronic journals.	
776	0	8	i| Print version: t| Journal of power sources x| 0378-7753 w| (DLC) 76647013 w| (OCoLC)2664681	
856	4	0	u| http://SK8ES4MC2L.search.serialssolutions.com/?V=1.0&L=SK8ES4MC2L&S=JCs&C=JOUROFPOWSO&T=marc	
910			a| CONSER online	
949			a| Electronic resource w| ASIS c| 1 i| 44133696-1001 l| ONLINE m| ONLINE r| Y s| Y t| ONLINE u| 4/20/2024 o| .STAFF. 360 MARC	

ASK A LIBRARIAN

PennState

Copyright @2019 The Pennsylvania State University. All rights reserved. Except where otherwise noted, this work is subject to a Creative Commons Attribution 4.0 license. Details and exceptions.

Legal Statements | PSU Hotlines

PENN STATE UNIVERSITY LIBRARIES

Libraries Home
Libraries Intranet (Staff Only)
Accessibility Help
Website Feedback
Policies and Guidelines
Staff Directory

(814) 865-6368

CONNECT WITH PENN STATE UNIVERSITY LIBRARIES

Facebook
Twitter
Instagram

Journal of power sources [electronic resource].

Uniform Title: Journal of power sources (Online)

Published: Lausanne : Elsevier Sequoia, [1976]-

Access Online

serialssolutions.com

ASK A LIBRARIAN

Dates of Publication and/or Sequential Designation:
Vol. 1, issue 1 (Dec. 1976)-

Subject(s):
Power resources—Periodicals
Power (Mechanics)—Periodicals

Genre(s):
Electronic journals

ISSN:
1873-2755

Publication Frequency:
24 issues a year, <2007->
Frequency varies, 1976-

Note:
Title from contents screen (ScienceDirect, viewed Mar. 9, 2007).

Special Numbering:
Some issues combined.

Technical Details:
Mode of access: World Wide Web.

View MARC record | catkey: 44133696

PennState

Copyright @2019 The Pennsylvania State University. All rights reserved. Except where otherwise noted, this work is subject to a Creative Commons Attribution 4.0 license. Details and exceptions.

Legal Statements | PSU Hotlines

PENN STATE UNIVERSITY LIBRARIES

Libraries Home (814) 865-6368
Libraries Intranet (Staff Only)
Accessibility Help
Website Feedback
Policies and Guidelines
Staff Directory

CONNECT WITH PENN STATE UNIVERSITY LIBRARIES

Facebook
Twitter
Instagram

ScienceDirect

Journal of Power Sources

Supports open access

15.9
CiteScore

9.2
Impact Factor

Submit your article

Guide for authors

Menu

Search in this journal

Volume 195, Issue 16

Pages 5155-5428 (15 August 2010)

Download full issue

Previous vol/issue

Next vol/issue

Receive an update when the latest issues in this journal are published

Sign in to set up alerts

Full text access

Editorial Board

Page CO2

View PDF

Fuel Cells: Science and Technology

Articles

Research article Full text access

Investigation of sheet resistance in thin-film mixed-conducting solid oxide fuel cell cathode test cells

Matthew E. Lynch, Meilin Liu

Pages 5155-5166

FEEDBACK

View PDF Article preview

Abstract

Abstract

Patterned and thin-film electrode experiments are effective in isolating or separating the complex charge and mass transport processes involved in the oxygen reduction reaction within and on the surface of a mixed-conducting solid oxide fuel cell cathode, making it possible to correlate electrochemical performance with electrode geometry, reaction pathway, and limiting steps. Very little information about either the impact of sheet resistance on global response or on effective design of current collector configuration to avoid sheet resistance has been reported to date, however. In this contribution, an empirical numerical model is presented to simulate sheet resistance under various material and catalytic parameters, current collector configurations, and other experimental factors in thin-film, mixed-conducting working electrodes. This model is used to provide general guidance for effective current collector placement by mapping in parameter space. In general, continuous crisscrossing metal lines, deposited through e.g. photolithography, provide the

Research article Full text access

Influence of carbon support microstructure on the polarization behavior of a polymer electrolyte membrane fuel cell membrane electrode assemblies

Abhishek Guha, Thomas A. Zawodzinski, David A. Schiraldi

Pages 5167-5175

View PDF Article preview

Abstract

Abstract

The influence of carbon support morphology on the polarization behavior of a PEM fuel cell membrane electrode assembly has been investigated in this communication. Nanometer sized platinum electrocatalyst particles were deposited on lower surface area fibrous (carbon nanofibers) and particulate carbon supports (carbon blacks) by the well-documented ethylene glycol route for supported electrocatalyst synthesis. These supported catalyst systems were subsequently utilized to prepare catalyst inks and membrane electrode assemblies (MEA) in conjunction with a perflurosulfonated ionomeric membrane-Nafion®. Level of liquid Nafion binder in the supported catalyst inks was varied and the ramifications of such a variation on polarization behavior of the MEA determined. The trend in polarization performance was found to be independent of the carbon support morphology in the various ink compositions. The two varieties of carbon supports were also mixed together in various weight ratios and platinum was deposited by the glycol

Research article Full text access

Evaluation of $Ba_{0.6}Sr_{0.4}Co_{0.9}Nb_{0.1}O_{3-\delta}$ mixed conductor as a cathode for intermediate-temperature oxygen-ionic solid-oxide fuel cells

Cheng Huang, Dengjie Chen, Ye Lin, Ran Ran, Zongping Shao

Pages 5176-5184

View PDF Article preview

Abstract

Abstract

A perovskite-type $Ba_{0.6}Sr_{0.4}Co_{0.9}Nb_{0.1}O_{3-\delta}$ (BSCN) oxide is investigated as the cathode material of oxygen-ionic solid-oxide fuel cells (SOFCs) with $Sm_{0.2}Ce_{0.8}O_{3-\delta}$ (SDC) electrolyte. Powder X-ray diffraction and SEM characterization demonstrate that solid phase reactions between BSCN and SDC are negligible at temperatures up to 1100 °C. The results of thermal-expansion and electrical conductivity measurements indicate the introduction of Ba^{2+} into the A-site of $SrCo_{0.9}N_{0.1}O_{3-\delta}$ (SCN) led to a decrease in the thermal-expansion coefficient (TEC) and electrical conductivity of the compound. A TEC of $14.4\times10^{-6}K^{-1}$ is observed for BSCN within a temperature range of 200–500 °C. The chemical diffusion coefficient (D_{chem}) and surface exchange constant (k_{ex}) of BSCN and SCN are obtained using an electrical conductivity relaxation technique and BSCN prove to have higher D_{chem} and k_{ex} than SCN. An area-specific resistance of 0.1 Ωcm^{-2} is achieved for BSCN cathodes at 600 °C based on symmetric cells test. Peak power density of ~1150 mW/cm^{-2} is

Research article Full text access

On the role of ultra-thin oxide cathode synthesis on the functionality of micro-solid oxide fuel cells: Structure, stress engineering and *in situ* observation of fuel cell membranes during operation

Bo-Kuai Lai, Kian Kerman, Shriram Ramanathan

Pages 5185-5196

View PDF Article preview

Abstract

Abstract

Microstructure and stresses in dense $La_{0.6}Sr_{0.4}Co_{0.8}Fe_{0.2}O_3$ (LSCF) ultra-thin films have been investigated to increase the physical thickness of crack-free cathodes and active area of thermo-mechanically robust micro-solid oxide fuel cell (μSOFC) membranes. Processing protocols employ low deposition rates to create a highly granular nanocrystalline microstructure in LSCF thin films and high substrate temperatures to produce linear temperature-dependent stress evolution that is dominated by compressive stresses in μSOFC membranes. Insight and trade-off on the synthesis are revealed by probing microstructure evolution and electrical conductivity in LSCF thin films, in addition to *in situ* monitoring of membrane deformation while measuring μSOFC performance at varying temperatures. From these studies, we were able to successfully fabricate failure-resistant square μSOFC (LSCF/YSZ/Pt) membranes with width of 250 μm and crack-free cathodes with thickness of ~70 nm. Peak power density of ~120 mW/cm^{-2} and open circuit voltage of ~0.6 V at

Short Communications

Short communication Full text access

Covalent-ionically cross-linked polyetheretherketone proton exchange membrane for direct methanol fuel cell

Hongze Luo, Guntars Vaivars, Mkhulu Mathe

Pages 5197-5200

View PDF Article preview

Abstract

Abstract

In this paper, the proton exchange membrane prepared by covalent-ionically cross-linking water soluble sulfonated–sulfinated poly(oxa-*p*-phenylene-3,3-phthalido-*p*-phenylene-oxa-*p*-phenylene-oxy-phenylene) (SsPEEK-WC) is reported. Compared with covalent cross-linked PEEK-WC membrane, this covalent-ionically cross-linked PEEK-WC membrane exhibits extremely reduced water uptake and methanol permeability, but just slightly sacrificed proton conductivity. The proton conductivity of the covalent-ionically cross-linked PEEK-WC membrane reaches to 2.1×10^{-2} S cm^{-1} at room temperature and 4.1×10^{-2} S cm^{-1} at 80 °C. The methanol permeability is 1.3×10^{-7} cm^2 s^{-1}, 10 times lower than that of Nafion® 117 membrane. The results suggest that the covalent-ionically cross-linked PEEK-WC membrane is a promising candidate for direct methanol fuel cell because of low methanol permeability and adequate proton conductivity.

Short communication Full text access

Performance of large-scale anode-supported solid oxide fuel cells with impregnated $La_{0.6}Sr_{0.4}Co_{0.2}Fe_{0.8}O_{3-\delta}$+$Y_2O_3$ stabilized ZrO_2 composite cathodes

Jing Chen, Fengli Liang, Dong Yan, Jian Pu, ... Li Jian

Pages 5201-5205

View PDF Article preview

Abstract

Abstract

Anode-supported planar solid oxide fuel cells (SOFCs) with an active area of 81 cm^2 (9 cm×9 cm) and nano-structured $La_{0.6}Sr_{0.4}Co_{0.2}Fe_{0.8}O_{3-\delta}$+$Y_2O_3$ stabilized ZrO_2 (LSCF+YSZ) composite cathodes are successfully fabricated by tape casting, screen printing, co-firing and solution impregnation, and tested using H_2 fuel and air oxidant at various flow rates. Maximum power densities of 437 and 473 mW cm^{-2} are achieved at 750 °C by loading 0.6 and 1.3 mg cm^{-2} of LSCF in the composite cathodes, respectively. The gas flow rates, particularly the air, have a significant effect on the cell performance. Cell performance degradation with time is also observed, which is considered to be associated with the growth and coalescence of the nanosized LSCF particles in the composite cathode. The use of the LSCF cathode in combination with YSZ electrolyte without a Gd-doped CeO_2 (GDC) buffer layer is proved to be applicable in large cells, even though the thermal stability of the nanosized LSCF needs to be further improved.

Fuel Cells: Engineering

Articles

Research article Full text access

Thermodynamic analysis of interactions between Ni-based solid oxide fuel cells (SOFC) anodes and trace species in a survey of coal syngas

Andrew Martinez, Kirk Gerdes, Randall Gemmen, James Poston
Pages 5206-5212

View PDF Article preview

Abstract

Abstract

A thermodynamic analysis was conducted to characterize the effects of trace contaminants in syngas derived from coal gasification on solid oxide fuel cell (SOFC) anode material. The effluents from 15 different gasification facilities were considered to assess the impact of fuel composition on anode susceptibility to contamination. For each syngas case, the study considers the magnitude of contaminant exposure resulting from operation of a warm gas cleanup unit at two different temperatures and operation of a nickel-based SOFC at three different temperatures. Contaminant elements arsenic (As), phosphorous (P), and antimony (Sb) are predicted to be present in warm gas cleanup effluent and will interact with the nickel (Ni) components of a SOFC anode. Phosphorous is the trace element found in the largest concentration of the three contaminants and is potentially the most detrimental. Poisoning was found to depend on the composition of the syngas as well as system operating conditions. Results for all trace elements tended to show

Research article Full text access

Numerical investigation of the impact of gas and cooling flow configurations on current and water distributions in a polymer membrane fuel cell through a pseudo-two-dimensional diphasic model

Sylvain Chupin, Thibaut Colinart, Sophie Didierjean, Yves Dubé, ... Olivier Lottin
Pages 5213-5227

View PDF Article preview

Abstract

Abstract

For optimal performances, proton exchange membrane fuel cells require fine water and thermal management. Accurate modelling of the physical phenomena occurring in the fuel cell is a key issue to improve fuel cell technology. Here, an analytic steady state diphasic 2D model of heat and mass transfer is presented. Through this model, the aim of this work is to study the influence of local events on the global performances of a fuel cell. A part of the complete model is a microscopic representation of the coupling between water transport and charge transfers in the electrodes. The thickness of the liquid layer around the reactive agglomerates is deduced from the saturation. The evolution of the quantity of water within the catalyst layer is monitored and its influence on the global performances of the cell is investigated. In gas diffusion layers (GDLs), liquid and vapour water transport through are computed regarding the temperature. The flow direction of cooling water modifies the current density distribution along the cell. The impact of the direction of air and

Research article Full text access

Improvement of water management in polymer electrolyte membrane fuel cell thanks to cathode cracks

Nicolas Karst, Vincent Faucheux, Audrey Martinent, Pierre Bouillon, Jean-Pierre Simonato
Pages 5228-5234

View PDF Article preview

Abstract

Abstract

The role of cathodic structure on water management was investigated for planar micro-air-breathing polymer electrolyte membrane fuel cells (PEMFCs). The electrical results demonstrate the possibility to decrease, with the same structure, both cell drying and cell flooding according to the environmental and operation conditions. Thanks to a simultaneous study of internal resistance and scanning electronic microscope (SEM) images, we demonstrate the advantageous influence of the presence of crack in cathodic catalytic layer on water management. On the one hand, the gold layer used as cathodic current collector is in contact with the electrolyte in the cracked zones which allows water maintenance within the electrolyte. It allows to decrease the cell drying and thus strongly increase the electrical performances. For cells operated in a 10% relative humidity atmosphere at 30 °C and at a potential of 0.5 V, the current density increases from 28 mA cm^{-2} to 188 mA cm^{-2} (+570%) for the cell with a cathodic cracked network. On the other hand, the reduction in

Research article Full text access

On the temperature distribution in polymer electrolyte fuel cells

J.G. Pharoah, O.S. Burheim
Pages 5235-5245

View PDF Article preview

Abstract

Abstract

This paper presents 2D thermal model of a fuel cell to elucidate some of the issues and important parameters with respect to temperature distributions in PEM fuel cells. A short review on various properties affecting the temperature profile and the heat production in the polymer electrolyte fuel cell is included. At an average current density of 1 A cm^{-2}, it is found that the maximum temperature of the MEA is elevated by between 4.5 and 15 K compared to the polarisation plate temperature. The smallest deviation corresponds to one dimensional transport, while the largest corresponds to the two dimensional transport considering anisotropic thermal conductivity. The two dimensional thermal model further predicts increased lost work. While most of the heat generation is allocated in the cathode, it is shown that the heat effect may be balanced by the water phase change in the anode. The most significant factor in determining the temperature distribution is the gas channel geometry (width and channel type), followed by the thermal conductivity of

Research article Full text access

Performance of carbon nanofiber supported Pd–Ni catalysts for electro-oxidation of ethanol in alkaline medium

T. Maiyalagan, Keith Scott
Pages 5246-5251

View PDF Article preview

Abstract

Abstract

Carbon nanofibers (CNF) supported Pd–Ni nanoparticles have been prepared by chemical reduction with $NaBH_4$ as a reducing agent. The Pd–Ni/CNF catalysts were characterized by X-ray diffraction (XRD), scanning electron microscopy (SEM), transmission electron microscopy (TEM) and electrochemical voltammetry analysis. TEM showed that the Pd–Ni particles were quite uniformly distributed on the surface of the carbon nanofiber with an average particle size of 4.0 nm. The electro-catalytic activity of the Pd–Ni/CNF for oxidation of ethanol was examined by cyclic voltammetry (CV). The onset potential was 200 mV lower and the peak current density four times higher for ethanol oxidation for Pd–Ni/CNF compared to that for Pd/C. The effect of an increase in temperature from 20 to 60 °C had a great effect on increasing the ethanol oxidation activity.

Research article Full text access

Stability and performance improvement of a polymer electrolyte membrane fuel cell stack by laser perforation of gas diffusion layers

Dietmar Gerteisen, Christian Sadeler
Pages 5252-5257

View PDF Article preview

Abstract

Abstract

The performance and stability of a hydrogen-driven polymer electrolyte membrane fuel cell stack (6-cell PEFC stack) are investigated with regard to pore flooding within the gas diffusion layers (GDLs). Two short stacks with various GDLs (Toray TGP-H-060 untreated and laser-perforated) were characterized at different operating conditions by several characterization techniques such as constant current load, polarization curve, chronoamperometry and chronovoltammetry. The experimental results reveal that the perforation of the cathode GDLs improves the water transport in the porous media and thus the performance as well as the stability of the operating stack in medium and high current density range. A reduced pore flooding is verified when using the customized laser-perforated GDLs. The GDL perforation has a huge potential to balance the inhomogeneous in-plane saturation conditions between the inlet and outlet area of the cell and to compensate to a certain degree the effects of temperature distribution within a stack

Research article Full text access

Influence of local porosity and local permeability on the performances of a polymer electrolyte membrane fuel cell

Tilda Akiki, Willy Charon, Marie-Christine Iltchev, Gilbert Accary, Raed Kouta
Pages 5258-5268

View PDF Article preview

Abstract

Abstract

In the literature, many models and studies focused on the steady-state aspect of fuel cell systems while their dynamic transient behavior is still a wide area of research. In the present paper, we study the effects of mechanical solicitations on the performance of a proton exchange membrane fuel cell as well as the coupling between the physico-chemical phenomena and the mechanical behavior. We first develop a finite element method to analyze the local porosity distribution and the local permeability distribution inside the gas diffusion layer induced by different pressures applied on deformable graphite or steel bipolar plates. Then, a multi-physical approach is carried out, taking into account the chemical phenomena and the effects of the mechanical compression of the fuel cell, more precisely the deformation of the gas diffusion layer, the changes in the physical properties and the mass transfer in the gas diffusion layer. The effects of this varying porosity and permeability fields on the polarization and on the power density curves are reported, and the

Research article Full text access

Effect of manufacturing processes on formability and surface topography of proton exchange membrane fuel cell metallic bipolar plates

Sasawat Mahabunphachai, Ömer Necati Cora, Muammer Koç
Pages 5269-5277

View PDF Article preview

Abstract

Abstract

Metallic bipolar plates in PEM fuel cells offer low-volume, low-mass and low-cost stack fabrication in addition to superior durability when compared to composite bipolar plates, which suffer due to their much higher thickness and less durability. This study aims to address the formability and surface topography issues of metallic bipolar plates fabricated by stamping and hydroforming technologies. Particular emphasis was given to process repeatability, surface topology, and dimensional quality of bipolar plates that would greatly affect the corrosion and contact resistance characteristics. Thin metal sheets of several alloys (i.e., SS304, SS316L, SS430, Ni270, Ti grades 1 and 2) were used in the fabrication experiments. SS304 and SS316L were shown to possess better formability when compared to other alloys that were used in this study, while SS430 and Ti grade 2 demonstrated the worst among all. Channel formability was observed to be greatly affected by the hydroforming pressure, while it does not differ much above certain level of stamping force. The

Research article Full text access

A numerical investigation on multi-phase transport phenomena in a proton exchange membrane fuel cell stack

Anh Dinh Le, Biao Zhou
Pages 5278-5291

View PDF Article preview

Abstract

Abstract

In this study, the simulation of a fuel cell stack is performed by applying a general numerical model with VOF method that has been successfully applied to single PEMFC model to investigate the fluid dynamics, mass transport, flooding phenomenon and the effects of liquid water on the stack performance. The performance of three single cells in series connection in the fuel cell stack is examined according to the presence of liquid water in different single cells. The distributions of fluid flow, species concentration and the current density are presented to illustrate the effects of liquid water on the performance of each single cell. The numerical results locate that the low distributions of species in the flooding cell certainly degrade the performance of this cell. Moreover, it can be seen that the performance of the flooding cell will significantly affect the whole stack performance since the values of average current density must be identical in all single cells

Research article Full text access

Improved modeling and understanding of diffusion-media wettability on polymer-electrolyte-fuel-cell performance

Adam Z. Weber
Pages 5292-5304

View PDF Article preview

Abstract

Abstract

A macroscopic-modeling methodology to account for the chemical and structural properties of fuel-cell diffusion media is developed. A previous model is updated to include for the first time the use of experimentally measured capillary pressure–saturation relationships through the introduction of a Gaussian contact-angle distribution into the property equations. The updated model is used to simulate various limiting-case scenarios of water and gas transport in fuel-cell diffusion media. Analysis of these results demonstrate that interfacial conditions are more important than bulk transport in these layers, where the associated mass-transfer resistance is the result of higher capillary pressures at the boundaries and the steepness of the capillary pressure–saturation relationship. The model is also used to examine the impact of a microporous layer, showing that it dominates the response of the overall diffusion medium. In addition, its primary mass-transfer-related effect is suggested to be limiting the water-injection sites into the more porous gas-diffusion layer

Research article Full text access

Degradation location study of proton exchange membrane at open circuit operation

Shaohua Xiao, Huamin Zhang, Cheng Bi, Yu Zhang, ... Xianfeng Li

Pages 5305-5311

View PDF Article preview

Abstract

Abstract

In order to investigate the location of the radical-initiated membrane degradation at open circuit operation, ceria (CeO_2) nanoparticles are firstly placed at different locations of the membranes to scavenge free radicals generated there. Scanning electron microscopy (SEM) is used to characterize cross-sectional morphology of membrane before and after the open circuit voltage (OCV) test. OCV decay rate is used as an indicator of membrane degradation rate. Composite membranes with CeO_2 nanoparticles facing anode or cathode show improved membrane durability than that of plain membrane in terms of OCV decay rate and cross-sectional morphology. CeO_2–Nafion composite membrane with the same thickness is subsequently proposed and it obtains the best durability. It is concluded that the chemical degradation at open circuit operation occurs at both sides of anode and cathode.

Research article Full text access

The preparation technique optimization of epoxy/compressed expanded graphite composite bipolar plates for proton exchange membrane fuel cells

Chao Du, Pingwen Ming, Ming Hou, Jie Fu, ... Baolian Yi

Pages 5312-5319

View PDF Article preview

Abstract

Abstract

Vacuum resin impregnation method has been used to prepare polymer/compressed expanded graphite (CEG) composite bipolar plates for proton exchange membrane fuel cells (PEMFCs). In this research, three different preparation techniques of the epoxy/CEG composite bipolar plate (Compression–Impregnation method, Impregnation–Compression method and Compression–Impregnation–Compression method) are optimized by the physical properties of the composite bipolar plates. The optimum conditions and the advantages/disadvantages of the different techniques are discussed respectively. Although having different characteristics, bipolar plates obtained by these three techniques can all meet the demands of PEMFC bipolar plates as long as the optimum conditions are selected. The Compression–Impregnation–Compression method is shown to be the optimum method because of the outstanding properties of the bipolar plates. Besides, the cell assembled with these optimum composite bipolar plates shows excellent stability after 200h durability testing

Research article Full text access

Detailed dynamic Solid Oxide Fuel Cell modeling for electrochemical impedance spectra simulation

Ph. Hofmann, K.D. Panopoulos
Pages 5320-5339

View PDF Article preview

Abstract

Abstract

This paper presents a detailed flexible mathematical model for planar solid oxide fuel cells (SOFCs), which allows the simulation of steady-state performance characteristics, i.e. voltage–current density (V–j) curves, and dynamic operation behavior, with a special capability of simulating electrochemical impedance spectroscopy (EIS). The model is based on physico-chemical governing equations coupled with a detailed multi-component gas diffusion mechanism (Dusty-Gas Model (DGM)) and a multi-step heterogeneous reaction mechanism implicitly accounting for the water-gas-shift (WGS), methane reforming and Boudouard reactions. Spatial discretization can be applied for 1D (button-cell approximation) up to quasi-3D (full size anode supported cell in cross-flow configuration) geometries and is resolved with the finite difference method (FDM). The model is built and implemented on the commercially available modeling and simulations platform gPROMS™. Different fuels based on hydrogen, methane and syngas with inert diluents are run. The model is

Short Communication

Short communication Full text access

Influence of anode thickness on the power output of solid oxide fuel cells with (La,Sr)(Co,Fe)-type cathode

Norbert H. Menzler, Vincent A.C. Haanappel
Pages 5340-5343

View PDF Article preview

Abstract

Abstract

The influence of the thickness of the anode (functional layer) on the power output of anode-supported solid oxide fuel cells with a lanthanum–strontium–cobalt–ferrite cathode was investigated. The anode was applied by vacuum slip casting and the thickness varied between 1 and 22 μm. All other material and microstructural parameters were kept constant. Single cells with dimensions of 50 mm × 50 mm and with an active cathode area of 40 mm × 40 mm were manufactured and tested in an alumina housing with air as oxidant and hydrogen with 3% water vapour as the fuel gas.

Results have shown that SOFCs with anodes between 1 and 13 μm have slightly better performance than those with thicker anodes (~1.7 A cm^{-2} versus 1.5 A cm^{-2} at 800 °C and 0.7 V). The current densities were discussed with respect to cell area specific resistance, helium leak rate of the half-cell, and microstructure.

Lithium Batteries: Science and Technology

Articles

Research article Full text access

Lithium oxalyldifluoroborate/carbonate electrolytes for $LiFePO_4$/artificial graphite lithium-ion cells

Jie Li, Keyu Xie, Yanqing Lai, Zhi'an Zhang, ... Yexiang Liu

Pages 5344-5350

View PDF Article preview

Abstract

Abstract

The electrolytes based on lithium oxalyldifluoroborate (LiODFB) and carbonates have been systematically investigated for $LiFePO_4$/artificial graphite (AG) cells, by ionic conductivity test and various electrochemical tests, such as cyclic voltammetry (CV), electrochemical impedance spectroscopy (EIS), and charge–discharge test. The conductivity of nine electrolytes as a function of solvent composition and LiODFB salt concentration has been studied. The coulombic efficiency of $LiFePO_4$/Li and AG/Li half cells with these electrolytes have also been compared. The results show that 1 M LiODFB EC/PC/DMC (1:1:3, v/v) electrolyte has a relatively higher conductivity (8.25 mS cm^{-1}) at 25 °C, with high coulombic efficiency, good kinetics characteristics and low interface resistance. With 1 M LiODFB EC/PC/DMC (1:1:3, v/v) electrolyte, $LiFePO_4$/AG cells exhibit excellent capacity retention ~92% and ~88% after 100 cycles at 25 °C and at elevated temperatures up to 65 °C, respectively; The $LiFePO_4$/AG cells also have good rate capability, the discharge capacity is

Research article Full text access

Preparation of C-$LiFePO_4$/polypyrrole lithium rechargeable cathode by consecutive potential steps electrodeposition

Iker Boyano, J. Alberto Blazquez, Iratxe de Meatza, Miguel Bengoechea, ... John B. Goodenough

Pages 5351-5359

View PDF Article preview

Abstract

Abstract

In this work carbon coated lithium iron phosphate (C-$LiFePO_4$)/polypyrrole (PPy) composite preparation has been carried out using electrochemical techniques. This composite has been deposited on a stainless steel mesh in order to use it as a cathode in a lithium-ion battery. When an oxidation potential is applied to the working electrode, the pyrrole monomer is polymerized and the C-$LiFePO_4$ particles are incorporated into the polymer matrix and bound to the polymer and mesh. An experimental procedure was performed in order to understand how the composite formation is carried out and what the oxidation state of the composite material is during the charge–discharge process. As the electrochemical method of synthesis has a big influence in the electrochemical properties of the polymer, the use of consecutive potential steps has been studied in order to improve the charge-storage capacity of the composite material. The influence on the final composite properties of the oxidation–deposition time and potential and the effect of the number of cycles has been

Research article Full text access

Multi-walled carbon nanotubes functionalized by carboxylic groups: Activation of TiO_2 (anatase) and phosphate olivines ($LiMnPO_4$; $LiFePO_4$) for electrochemical Li-storage

Ladislav Kavan, Revathi Bacsa, Meltem Tunckol, Philippe Serp, ... Michael Graetzel

Pages 5360-5369

View PDF Article preview

Abstract

Abstract

Multi-walled carbon nanotubes functionalized by carboxylic groups, exhibit better affinity towards TiO_2 (P90, Degussa) as compared to that of pristine nanotubes. Also the electrochemical performance of TiO_2 is improved by nanotube networking, but the Li-storage capacity of TiO_2 is unchanged. Whereas the composite of TiO_2 with non-functionalized nanotubes demonstrates simple superposition of the behavior of pure components, the composite with functionalized nanotubes shows unique faradaic pseudocapacitance which is specific for this composite only. The surface functionalization of nanotubes enhances charge storage capacity and reversibility of a composite with $LiMnPO_4$ (olivine), but mediates also the electrolyte breakdown at potentials >4.2V. Whereas the electrochemical activation of $LiMnPO_4$ (olivine) by functionalized nanotubes is quite modest, excellent performance was found for $LiFePO_4$ (olivine) in composite materials containing only 2wt% of functionalized nanotubes

Short Communications

Short communication Full text access

Effect of ethanol-assisted electrode fabrication on the performance of silicon anodes

Sigita Urbonaite, Ida Baglien, David Ensling, Kristina Edström

Pages 5370-5373

View PDF Article preview

Abstract

Abstract

The performance of high-silicon-content anodes was tested as a function of silicon particle-size (44μm, 1.8μm and 70–100nm), surface pre-treatment and solvent chosen for anode preparation. Two simple procedures, leading to significant improvements in electrode performance are reported. First, pre-treatment of nano-Si in ethanol which unexpectedly yields functionalised surfaces improving cycling stability. Second, the use of a 30:70 solution of ethanol and water to dissolve the CMC-binder for the electrode preparation boosts specific battery capacity. Ethanol pre-treatment of nano-Si also resulted in improved adhesion of the electrode to the current collector as well as in de-agglomeration of nano-Si powder. All these treatments improved capacity stability during cycling. Changes in surface chemistry of nano-Si before and after ethanol treatment have been analysed by XPS. A stable capacity of about 1630mAhg^{-1} was obtained after 25 cycles for an electrode containing 80% silicon using ethanol during electrode coating preparation

Short communication Full text access

Temperature-controlled microwave solid-state synthesis of $Li_3V_2(PO_4)_3$ as cathode materials for lithium batteries

Gang Yang, Haidong Liu, Hongmei Ji, Zhongzhong Chen, Xuefan Jiang
Pages 5374-5378

View PDF Article preview

Abstract

Abstract

Monoclinic $Li_3V_2(PO_4)_3$ can be rapidly synthesized at 750 °C for 5 min (MW5m) by using temperature-controlled microwave solid-state synthesis method (TCMS). The carbon-free sample MW5m presents well electrochemical properties. In the cut-off voltage 3.0–4.3, MW5m presents a charge capacity 132 mAhg^{-1}, almost equivalent to the reversible cycling of two lithium ions per $Li_3V_2(PO_4)_3$ formula unit (133 mAhg^{-1}), and discharge capacity 126.4 mAhg^{-1}. In the cut-off voltage 3.0–4.8 V, MW5m shows an initial discharge capacity of 183.4 mAhg^{-1}, near to the theoretical discharge capacity. In the cycle performance, the capacity fade of $Li_3V_2(PO_4)_3$ is dependent on the cut-off voltage and the preparation method.

Short communication Full text access

Fe_3O_4 submicron spheroids as anode materials for lithium-ion batteries with stable and high electrochemical performance

Suqing Wang, Jingying Zhang, Chunhua Chen
Pages 5379-5381

View PDF Article preview

Abstract

Abstract

A magnetite (Fe_3O_4) powder composed of uniform sub-micrometer spherical particles has been successfully synthesized by a hydrothermal method at low temperature. X-ray diffraction, scanning electron microscopy, transmission electron microscopy and galvanostatic cell cycling are employed to characterize the structure and electrochemical performance of the as-prepared Fe_3O_4 spheroids. The magnetite shows a stable and reversible capacity of over 900 mAhg^{-1} during up to 60 cycles and good rate capability. The experimental results suggest that the Fe_3O_4 synthesized by this method is a promising anode material for high energy-density lithium-ion batteries.

Short communication Full text access

In situ synthesis of ultra-fine, porous, tin oxide-carbon nanocomposites via a molten salt method for lithium-ion batteries

Bin Liu, Zai Ping Guo, Guodong Du, Yanna Nuli, ... Dianzeng Jia

Pages 5382-5386

View PDF Article preview

Abstract

Abstract

Ultra-fine, porous, tin oxide–carbon (SnO_2/C) nanocomposites are fabricated by a molten salt method at 300 °C, and malic acid is decomposed as the carbon source. In situ synthesis is favourable for the combination of carbon and SnO_2. The structure and morphology are confirmed by X-ray diffraction analysis, specific surface-area measurements, and transmission electron microscopy (TEM). Examination of TEM images reveals that the SnO_2 nanoparticles are embedded in the carbon matrix, with sizes between 2 and 5 nm. The electrochemical measurements show that the nanocomposite delivers a high capacity with good capacity retention as an anode material for lithium-ion batteries, due to the combination of the ultra-fine porous structure and the carbon component.

Lithium Batteries: Engineering

Short Communication

Short communication Full text access

Continuity and performance in composite electrodes

Guoying Chen, Thomas J. Richardson

Pages 5387-5390

View PDF Article preview

Abstract

Abstract

It is shown that the rate performance of a lithium battery composite electrode may be compromised by poor internal connectivity due to defects and inhomogeneities introduced during electrode fabrication or subsequent handling. Application of a thin conductive coating to the top surface of the electrode or to the separator surface in contact with the electrode improves the performance by providing alternative current paths to partially isolated particles of electroactive material. Mechanistic implications are discussed and strategies for improvement in electrode design and fabrication are presented.

Other Electrochemical Power Sources: Science and Technology

Article

Research article Full text access

Synthesis of new low band gap dyes with BF_2–azopyrrole complex and their use for dye-sensitized solar cells

John A. Mikroyannidis, M.S. Roy, G.D. Sharma

Pages 5391-5398

View PDF Article preview

Abstract

Abstract

The diazonium salt derived from 4-aminobenzoic acid, 4-aminophenol or 2-aminophenol reacted with half equivalent of pyrrole to afford symmetrical 2,5-bisazopyrroles. They reacted subsequently with boron trifluoride in the presence of triethylamine to afford the corresponding BF_2–azopyrrole complexes **D1**, **D2** and **D3** respectively. They were soluble and stable in nonprotic solvents such as chloroform, dichloromethane and tetrahydrofuran but unstable in protic solvents such as ethanol. Their absorption spectra were broad with optical band gap of 1.49–1.70 eV. Among these dyes **D2** displayed the broader absorption spectrum with low band gap E_g^{opt} of 1.49 eV. We have utilized these complexes as photosensitizers for quasi solid state dye-sensitized solar cells (DSSCs) and achieved power conversion efficiency in the range of 4.0–6.0%. We have also found that the co-adsorption of citric acid hindered the formation of dye aggregates and might improve the electron injection efficiency leading to an enhancement in short circuit photocurrent. This work

Other Electrochemical Power Sources: Engineering

Article

Research article Full text access

Analysis of plug-in hybrid electric vehicle utility factors

Thomas H. Bradley, Casey W. Quinn

Pages 5399-5408

View PDF Article preview

Abstract

Abstract

Plug-in hybrid electric vehicles (PHEVs) are hybrid electric vehicles that can be fueled from both conventional liquid fuels and grid electricity. To represent the total contribution of both of these fuels to the operation, energy use, and environmental impacts of PHEVs, researchers have developed the concept of the utility factor. As standardized in documents such as SAE J1711 and SAE J2841, the utility factor represents the proportion of vehicle distance travelled that can be allocated to a vehicle test condition so as to represent the real-world driving habits of a vehicle fleet. These standards must be used with care so that the results are understood within the context of the assumptions implicit in the standardized utility factors. This study analyzes and derives alternatives to the standard utility factors from the 2001 National Highway Transportation Survey, so as to understand the sensitivity of PHEV performance to assumptions regarding charging frequency, vehicle characteristics, driver characteristics, and means of defining the utility factor

Other Electrochemical Power Sources: Applications

Article

Research article Full text access

Emissions impacts of plug-in hybrid electric vehicle deployment on the U.S. western grid

Karel H. Jansen, Tim M. Brown, G. Scott Samuelsen

Pages 5409-5416

View PDF Article preview

Abstract

Abstract

The constantly evolving western grid of the United States is characterized by complex generation dispatch based on economics, contractual agreements, and regulations. The future electrification of transportation via plug-in electric vehicles calls for an energy and emissions analysis of electric vehicle (EV) penetration scenarios based on realistic resource dispatch. A resource dispatch and emissions model for the western grid is developed and a baseline case is modeled. Results are compared with recorded data to validate the model and provide confidence in the analysis of EV-grid interaction outlooks. A modeled dispatch approach, based on a correlation between actual historical dispatch and system load data, is exercised to show the impacts (emission intensity, temporally resolved load demand) associated with EV penetration on the western grid. The plug-in hybrid electric vehicle (PHEV) and selected charging scenarios are the focus for the analysis. The results reveal that (1) a correlation between system load and resource group capacity

Supercapacitors: Science and Technology

Short Communication

Short communication Full text access

Preparation and electrochemical capacitance performances of super-hydrophilic conducting polyaniline

Xingwei Li, Xiaohan Li, Na Dai, Gengchao Wang, Zhun Wang
Pages 5417-5421

View PDF Article preview

Abstract

Abstract

Super-hydrophilic conducting polyaniline was prepared by surface modification of polyaniline using tetraethyl orthosilicate in water/ethanol solution, whereas its conductivity was 4.16 Scm^{-1} at 25 °C. And its electrochemical capacitance performances as an electrode material were evaluated by the cyclic voltammetry and galvanostatic charge/discharge test in 0.1 M H_2SO_4 aqueous solution. Its initial specific capacitance was 500 Fg^{-1} at a constant current density of 1.5 Ag^{-1}, and the capacitance still reached about 400 Fg^{-1} after 5000 consecutive cycles. Moreover, its capacitance retention ratio was circa 70% with the growth of current densities from 1.5 to 20 Ag^{-1}, indicating excellent rate capability. It would be a promising electrode material for aqueous redox supercapacitors.

Photo Electrochemical Cells

Short Communication

Short communication Full text access

Tungsten oxide bilayer electrodes for photoelectrochemical cells

Sung Jong Yoo, Seong Uk Yun, Yung-Eun Sung, Kwang-Soon Ahn
Pages 5422-5425

View PDF Article preview

Abstract

Abstract

WO_3 bilayer electrodes composed of WO_3 top and bottom layers are designed for photoelectrochemical cells (PECs). The bottom layers are sputter-deposited at a high temperature (773 K) that leads to large grains and suitable electrical pathways for carrier collection. The top layer is deposited at a low temperature (573 K) and consists of small grains, which give rise to large electrochemical reaction sites. The bilayer electrodes give a significant enhancement in PEC performance compared with WO_3 monolayer electrodes deposited at 573 or 773 K, because of a combination of favourable effects.

Erratum Full text access

Erratum to “Corrosion resistance characteristics of stamped and hydroformed PEMFC metallic bipolar plates” [J. Power Sources 195 (11) (2010) 3546–3552]

F. Dundar, Ender Dur, S. Mahabunphachai, Muammer Koc

Page 5426

View PDF

Erratum Full text access

Corrigendum to “Stable and high energy generation by a strain of *Bacillus subtilis* in a microbial fuel cell” [J. Power Sources 190 (2) (2009) 258–263]

Vanita Roshan Nimje, Chien-Yen Chen, Chien-Cheng Chen, Jiin-Shuh Jean, ... Jia-Lia Chen

Pages 5427-5428

View PDF

Previous vol/issue Next vol/issue

ISSN: 0378-7753

Copyright © 2024 Elsevier B.V. All rights are reserved, including those for text and data mining, AI training, and similar technologies.

ELSEVIER

All content on this site: Copyright © 2024 Elsevier B.V., its licensors, and contributors. All rights are reserved, including those for text and data mining, AI training, and similar technologies. For all open access content, the Creative Commons licensing terms apply.

RELX™

APPENDIX KAVAN02

Journal of Power Sources 195 (2010) 5360–5369

Contents lists available at ScienceDirect

Journal of Power Sources

journal homepage: www.elsevier.com/locate/jpowsour

Multi-walled carbon nanotubes functionalized by carboxylic groups: Activation of TiO_2 (anatase) and phosphate olivines ($LiMnPO_4$; $LiFePO_4$) for electrochemical Li-storage

Ladislav Kavan[a,*], Revathi Bacsa[b], Meltem Tunckol[b], Philippe Serp[b], Shaik M. Zakeeruddin[c], Florian Le Formal[c], Marketa Zukalova[a], Michael Graetzel[c]

[a] J. Heyrovský Institute of Physical Chemistry, v.v.i., Academy of Sciences of the Czech Republic, Dolejškova 3, CZ-18223 Prague 8, Czech Republic
[b] Laboratoire de Chimie de Coordination, UPR CNRS 8241, composante ENSIACET, Université de Toulouse UPS-INP-LCC 4, Allée Emile Monso, BP 74233, 31432, Toulouse, France
[c] Laboratoire de Photonique et Interfaces, EPFL, Ecublens, CH-1015 Lausanne, Switzerland

ARTICLE INFO

Article history:
Received 18 November 2009
Received in revised form 9 February 2010
Accepted 6 March 2010
Available online 12 March 2010

Keywords:
Multi-walled carbon nanotubes
Titanium dioxide
Phosphate olivines
Lithium storage

ABSTRACT

Multi-walled carbon nanotubes functionalized by carboxylic groups, exhibit better affinity towards TiO_2 (P90, Degussa) as compared to that of pristine nanotubes. Also the electrochemical performance of TiO_2 is improved by nanotube networking, but the Li-storage capacity of TiO_2 is unchanged. Whereas the composite of TiO_2 with non-functionalized nanotubes demonstrates simple superposition of the behavior of pure components, the composite with functionalized nanotubes shows unique faradaic pseudocapacitance which is specific for this composite only. The surface functionalization of nanotubes enhances charge storage capacity and reversibility of a composite with $LiMnPO_4$ (olivine), but mediates also the electrolyte breakdown at potentials >4.2 V. Whereas the electrochemical activation of $LiMnPO_4$ (olivine) by functionalized nanotubes is quite modest, excellent performance was found for $LiFePO_4$ (olivine) in composite materials containing only 2 wt% of functionalized nanotubes.

© 2010 Elsevier B.V. All rights reserved.

1. Introduction

Carbon nanotubes form conductive composites with inorganic nanocrystals (for recent review see Ref. [1]). Compared to single-wall carbon nanotubes (SWNT) the multi-walled carbon nanotubes (MWNT) are cheaper, mechanically more robust and their electrical conductivity is less affected by chemical functionalization. Composite materials of MWNT with titanium dioxide have been investigated for application in photocatalysis [2–6] including photocatalytic hydrogen generation [7] and dye-sensitized solar cells [8–11]. In these applications, the beneficial role of MWNT is assumed to consist in improved separation of photogenerated charges, but very low MWNT concentrations (<1 wt%) are required to avoid charge recombination with the electrolyte in dye-sensitized solar cells [8–11]. Improved separation of photogenerated electrons/holes was also demonstrated in solar cells based on band-gap excitation of TiO_2 dispersed on SWNT [12]. The electrochemical lithium storage in carbon nanotube/TiO_2 composites has been studied, too [13–17], reflecting the fact that TiO_2 (especially anatase [18–22], TiO_2(B) [18,23–25] and rutile [18,20,26]) belong to the top interesting host structures for lithium insertion. These studies confirmed in unison that the electrochemical activity of the composite TiO_2/nanotubes is improved compared to that of the parent pure TiO_2 [13–17]. Some authors reported on significantly enhanced Li-storage capacity of the TiO_2/MWNT nanocomposite [13,15], but others [14,16,17] did not support this observation.

From the viewpoint of electrochemical lithium storage, the phosphate olivines [27], *viz.* $LiMPO_4$ (M = Fe, Mn) have been extensively studied in the past. They are promising cathode materials for Li-ion batteries due to high safety, low cost and environmental tolerability. However, their poor electrical conductivity is a crucial issue to be addressed [28] either by doping [29] or by surface coating with elemental carbon [30,31]. The conductivity problem is considerably more significant for $LiMnPO_4$ (conductivity of $\approx 10^{-14}$ S cm^{-1} compared to $\approx 10^{-9}$ S cm^{-1} for $LiFePO_4$) [32] but optimization of the synthesis, that is the formation of carbon coating via ball-milling, provided reasonably active materials, too [33,34].

The effect of MWNT on improvement of the performance of $LiFePO_4$ has been reported by several studies in the past [32,35–42]. The synthetic strategies range from simple mixing [32,36,37,40,41], ball-milling [35,42], hydrothermal synthesis [38], in situ formation of MWNT from ferrocene [39] up to a bio-inspired route, that is a gene manipulation, which was used to align $LiFePO_4$ with SWNT [43]. An analogous electrochemical activation of $LiMnPO_4$ in a com-

* Corresponding author. Tel.: +420 2 6605 3975; fax: +420 2 8658 2307.
E-mail address: kavan@jh-inst.cas.cz (L. Kavan).

0378-7753/$ – see front matter © 2010 Elsevier B.V. All rights reserved.
doi:10.1016/j.jpowsour.2010.03.028

posite with MWNT was reported only recently [32]. In this case, the improvement of charging rate and capacity was quite modest [32], and not comparable to that of the optimized materials, fabricated via ball milling with carbon black [33,34].

The surface oxidation of carbon nanotubes by HNO_3 [6,8,10,15,16,32,37,41,44], H_2SO_4/HNO_3 [4] or H_2O_2 [9], producing among other groups also carboxyls, was sometimes mentioned to improve the anchoring of TiO_2 [4,6,8–10,15,16,44] or $LiMPO_4$ [32,37,41]. In the first case, there is a clear analogy with the strong interaction of carboxyl-containing molecules (Ru-bipyridine dyes) with the TiO_2 surface, which is crucial in dye-sensitized solar cells [10]. However, there are also reports that the oxidative functionalization is not necessary for anchoring to TiO_2, because the pristine MWNT behave similarly [15]. The interaction of carboxyls with phosphate olivine surface is less understood, but certainly important, too [45,46]. To the best of our knowledge, there is no systematic study of these contradictory issues, although detailed understanding is desirable of the MWNT functionalization (by surface oxidation forming carboxyls) for optimum attachment of MWNT towards titania or olivine surfaces.

This was the central motivation for the study reported here. A second argument for deeper investigation of these composites is based on our previous experience with a supramolecular assembly of SWNT with carboxyl-containing Ru–bipyridine complex [45–48]. This assembly offers unique electrochemical activation of $LiFePO_4$ called 'nanotube wiring' [45,46]. The advantage of our nanotube wiring consists in the fact, that it keeps the amount of conductive additives in the active electrode material at its natural minimum (≈0.04 wt% of carbon in $LiFePO_4$). This is important for optimization of Li-ion batteries. The reason is that the electrode materials, *viz*. olivines or TiO_2 [21,22] require *ca*. 10–20 wt% of graphitic carbon to be added. However, graphite does not contribute to the faradaic reaction in the cathode, but presents ballast, decreasing the charge (energy) density of the composite electrode in the same proportion. Obviously, simple oxidation of MWNT is an attractive and cheap alternative to our 'nanotube wiring' effect [45,46] for practical Li-ion batteries. Since TiO_2 is a prospective anode material, and $LiMPO_4$ olivines are promising cathode materials, concerted study of the interaction of MWNT with these three selected materials at defined comparable conditions is relevant for the development of high-power Li-ion batteries.

2. Experimental

Multi-walled carbon nanotubes were prepared from ethylene gas by chemical vapor deposition. The synthesis was carried out in a fluidized bed reactor, and Fe nanoparticles supported on alumina served as catalyst. Details on the reactor configuration and preparation of the catalyst can be found elsewhere [49]. The catalyst was removed by boiling with diluted sulfuric acid (50%) at 140 °C for 3 h after which the nanotubes were filtered when hot by a glass frit followed by washing with hot water and drying at 120 °C. The extraction of catalyst was followed by inductively-coupled mass spectrometry (ICP-MS) analysis, which gave the Al content between 200 and 500 ppm for various samples. For oxidative functionalization, 1 g of purified nanotubes was mixed with 50 mL of 65% HNO_3 and refluxed for 3 h at 120 °C under stirring. The nanotubes were filtered on a glass frit, washed with water until the filtrate reached a pH of 6, and dried at 120 °C for 48 h. The non-functionalized blank material is abbreviated MWNT-bl and the material functionalized by oxidation with HNO_3 is coded MWNT-ox. The extent of functionalization was determined by titration with a freshly prepared aqueous solution of NaOH (0.05 M) as in Ref. [50]. The amount of acid groups in the nanotubes was found to be 2.54×10^{-4} mol g^{-1} in MWNT-ox, and close to 0 in MWNT-bl.

Titanium dioxide P90 (from Degussa AG, Germany) powder had a BET (Brunauer–Emmett–Teller) area of 90 m^2 g^{-1} (rutile/anatase mixture with >90% anatase, average anatase particle size 13 nm). The carbon black Ketjenblack EC-600 was purchased from AkzoNobel. According to the manufacturer's specification, it had an electrical resistivity of 0.01–0.1 Ω cm and the BET specific surface area of 1250 m^2 g^{-1}. Another comparative material was medium-functionalized sample, abbreviated MWNT-mox, which was prepared from MWNT-bl by oxidation with 65%-HNO_3 similarly to MWNT-ox (see above). The titration analysis with 0.05 M NaOH gave the amount of acid groups to be 1.14×10^{-4} mol g^{-1} in MWNT-mox. The carbon-free olivines, $LiFePO_4$ and $LiMnPO_4$ were obtained from High Power Lithium, SA, Switzerland. The nitrogen adsorption isotherms indicated the BET surface areas as of 9 m^2 g^{-1} (for $LiFePO_4$) and 35 m^2 g^{-1} (for $LiMnPO_4$). The latter material was prepared *via* the "polyol" route, and consisted of platelets oriented in the *a*–*c* plane of the olivine lattice [33].

Nanotubes were dispersed in water under short sonication in an ultrasonic bath. To this solution a powder material (TiO_2, $LiMnPO_4$ or $LiFePO_4$) was added (in a proportion of 1–10 wt% of nanotubes in the mixture) and stirred overnight. The suspension was subsequently evaporated to dryness. The electrodes were prepared as follows: powder precursor material, either pure or carbon-containing (see above) was mixed with 5 wt% of polyvinylidene fluoride (PVDF) dissolved in N-methyl-2-pyrrolidone. The resulting slurry was diluted with N-methyl-2-pyrrolidone until a consistence of viscous paste, and then doctor-bladed onto F-doped conducting glass (FTO; TEC 15 from Libbey-Owens-Ford 15 Ω sq^{-1}). The film was cut into smaller pieces of 0.8–1 cm^2 active area, and dried at 100 °C in vacuum. Uncovered area at the edge of the FTO support served for making an electrical contact. The film's mass was between ca. 0.2–1 mg cm^{-2}.

SEM images were obtained using FESEM Philips XL30 FEG instrument. Infrared spectra were recorded on a Perkin-Elmer 1710 Fourier transform spectrophotometer (FTIR) using KBr pellets. ATR-FTIR spectra were measured using a FTS 7000 FTIR spectrometer (Digilab, USA). The spectra were accumulated with the diamond anvil ATR accessory, while the sample powder was pressed against the diamond window. Spectra were derived from 64 scans at a resolution of 2 cm^{-1}.

Electrochemical experiments employed an Autolab PGSTAT potentiostat (Ecochemie) controlled by the GPES 4 software. The electrolyte solution was 1 mol L^{-1} $LiPF_6$ in ethylene carbonate + dimethylcarbonate (EC/DMC; 1/1; w). The reference and counter electrodes were from Li-metal, hence all potentials are quoted against the Li/Li^+ reference electrode in this medium. All electrochemical measurements were carried out in a glove box under Ar-atmosphere.

3. Results and discussion

Fig. 1 shows cyclic voltammogram of thin-film electrode from pure non-functionalized nanotubes, MWNT-bl and the functionalized nanotubes, MWNT-ox. The voltammogram of MWNT-bl confirms an almost ideal double-layer charging in a broad window of electrochemical potentials. Therefore, the voltammetric currents scale with the first power of scan rate, ν as it is expected for capacitive charging:

$$I = \frac{dQ}{dt} = C_{dl} \times \frac{dE}{dt} = C_{dl}\nu, \quad (1)$$

Q is the voltammetric charge, $dE/dt = \nu$ is the scan rate and C_{dl} is the double-layer capacitance. Hence, if we divide the experimental currents by the scan rate and the mass of the electroactive material (m, cf. Fig. 1), we can estimate the specific capacitance, C of our nanotube sample. The found values (averaged from sev-

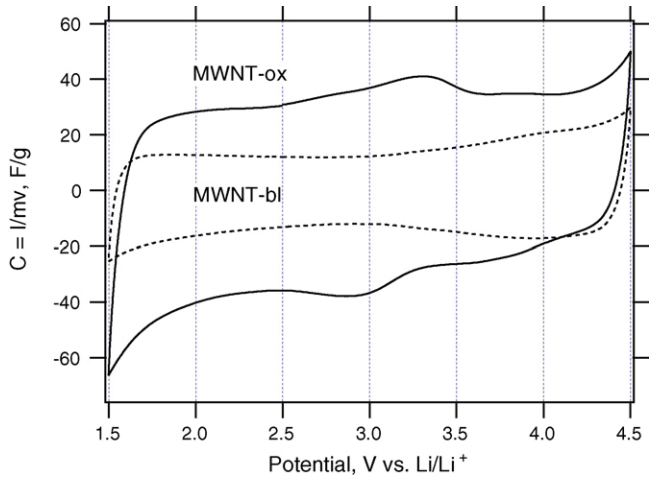


Fig. 1. Cyclic voltammograms of thin film electrodes from pure multi-walled carbon nanotubes, MWNT-bl (dashed curve) and functionalized, MWNT-ox (full curve). Scan rate 0.1 V/s. The current is divided by the scan rate and by the mass of nanotubes in the film, which was 0.26 or 0.22 mg cm^{-2} for MWNT-ox or MWNT-bl, respectively.

eral parallel experiments and varying scan rates) were 12 and 31 $F g^{-1}$ for the MWNT-bl and MWNT-ox, respectively. These capacitances fall among typical values for multi-walled carbon nanotubes in organic electrolyte solutions [51–54]. The MWNT-ox material exhibits characteristic pair of peaks at the formal potential of ca. 3.1 V vs. Li/Li^+. It can be assigned to reversible redox processes in surface oxygen-containing groups [51–56] such as:

$$> C{=}O + e^- \leftrightarrow C{-}O^- \quad (2)$$

which are considered faradaic pseudocapacitance.

The studied materials, *viz.* MWNT-ox and MWNT-bl exhibit significantly different solubility in water and interaction with TiO_2. The first material, MWNT-ox easily dissolves in water to form a black solution, which is stable against flocculation for months at room temperature. Mixing of this solution with TiO_2 (P90) causes immediate blackening of the titania powder and discoloration of the supernatant. In the second case, these effects are not seen: MWNT-bl is insoluble in water and there is only slight coloration of P90 by aqueous suspension of MWNT-bl.

Also the morphology of composites made from these precursors is different. Fig. 2 shows the SEM images of thin film electrodes from TiO_2 (P90), MWNT-ox and the composites TiO_2/MWNT-bl and TiO_2/MWNT-ox; in both cases the concentration of nanotubes is 10 wt%. For the MWNT-ox (right bottom chart), the interaction of nanotubes with titania is excellent. All nanotubes are covered with individual nanocrystals of P90 in a homogeneous nanocomposite. On the other hand, MWNT-bl makes a cracked structure, in which P90 is heavily agglomerated into micron-sized particles, and many 'naked' nanotubes are seen in-between the agglomerates. This morphology is similar to that reported by Tumcharen et al. [11] for pristine multi-walled nanotubes. Presumably, MWNT-bl interact with TiO_2 through small number of defects, and the naked parts of nanotubes are hydrophobic, defect-free areas on the MWNT-bl surface. Obviously, and in contrast to the work of Zeng et al. [15] our data on nanotubes/TiO_2(P90) support the

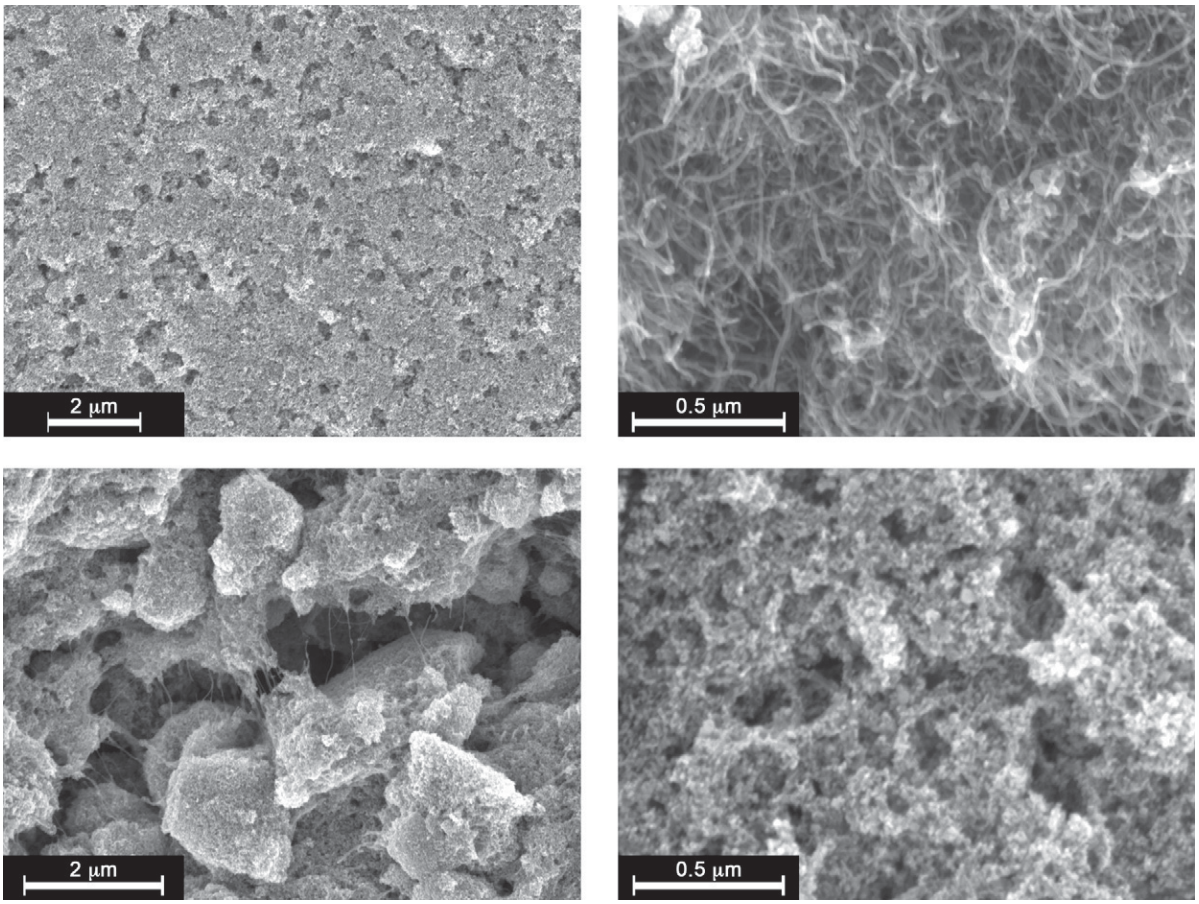


Fig. 2. Scanning electron microscopy images of thin film electrodes from P90 titanium dioxide. (Top left) Pure P90, scale bar 2 μm. (Top right) pure functionalized nanotubes MWNT-ox, scale bar 0.5 μm. (Bottom left) P90 in a composite with 10 wt% of non-functionalized nanotubes MWNT-bl, scale bar 2 μm. (Bottom right) P90 in a composite with 10 wt% of functionalized MWNT-ox, scale bar 0.5 μm.

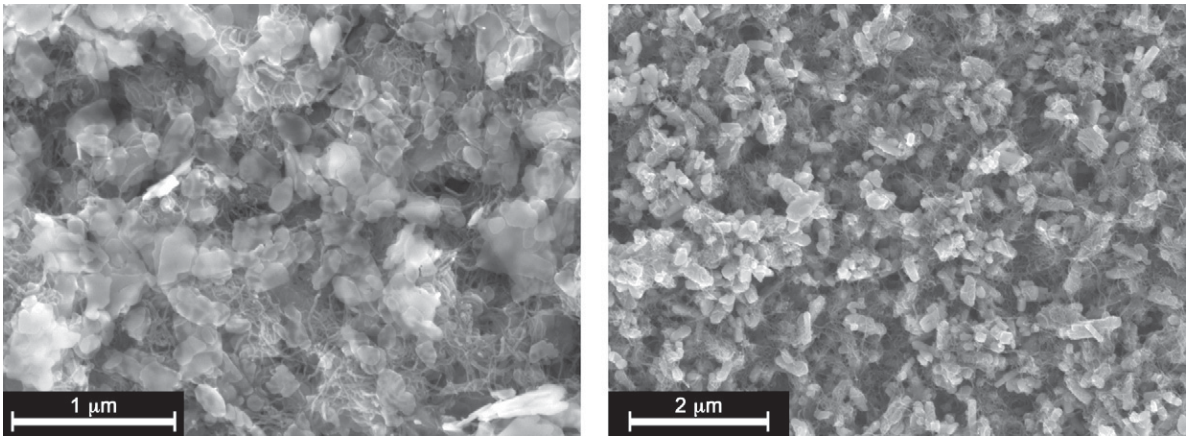


Fig. 3. Scanning electron microscopy images of thin film electrodes from phosphate olivines in a composite with 10 wt% of functionalized nanotubes, MWNT-ox. (Left) Composite with $LiMnPO_4$, scale bar 1 μm. (Right) Composite with $LiFePO_4$ scale bar 2 μm.

idea that oxidative functionalization through HNO_3 is crucial for proper anchoring of nanotubes towards TiO_2. The second message of Fig. 2 is that industrial powder (P90) is a good source of nanocrystals which spontaneously self-assemble on the nanotube surface. This information is important, because previous studies related to nanoparticles grown by laboratory protocols [2–10,13–17].

Fig. 3 shows the morphological features of our olivine/MWNT-ox composites (10 wt% MWNT-ox). In contrast to the structure of P90/MWNT-ox (Fig. 2) the naked nanotubes are easily recognized between the individual crystals of $LiMnPO_4$ (Fig. 3, left chart) as well as between $LiFePO_4$ crystals (Fig. 3, right chart). Two reasons might account for this difference. First, the olivine crystals are typically hundreds of nm in size, whereas the P90 crystals are ca. 10 nm in size. Hence, self-assembling of 10 nm sized crystals on the nanotube, having diameter of ca. 10 nm is feasible, but this kind of packing is hardly achievable with larger crystals. Second, the interaction of –COOH with phosphate surface might be less efficient, than the interaction of carboxyls with titania [10].

Fig. 4 (left panel) shows the FTIR spectra of MWNT-bl and MWNT-ox in KBr pellets. MWNT-ox exhibits the presence of a new band at 1710 cm^{-1} that is attributed to the C=O vibration of the carboxylic groups introduced by oxidative functionalization. The other intense IR band at 1570 cm^{-1} is attributed to the skeletal in-plane vibration of multi-walled nanotube. While MWNT-bl was almost free from surface carboxyls, the sample MWNT-ox contained 2.54×10^{-4} mol g^{-1} acidic groups as determined by titration analysis (see Section 2). The amount of atomic oxygen present on the MWNT-ox surface was also analyzed by X-ray photoelectron spectroscopy (data not shown) that gave a value of 7%. These results are in accordance with those reported earlier for functionalized carbon nanotubes [50]. The sample MWNT-bl further exhibits strong absorption features between 900 and 1300 cm^{-1} with a broad peak at 1110 cm^{-1}. These absorption bands presumably arise from aluminum sulfate impurity in the sample [57] which is introduced during the removal of alumina-supported catalyst by sulfuric acid treatment. The ICP-MS analysis gave the residual concentration of aluminum sulfate in MWNT-bl to be less than 500 ppm (see Section 2). The impurity peaks are not observed in the sample MWNT-ox, hence, they disappear as a result of nitric acid treatment and subsequent washing. In the region around 1200 cm^{-1}, we can also assume the presence of some weak IR bands of C–O and C–C stretching vibrations [57,58]. Although the carbon skeleton can decay and change its vibrational structure as a result of functionalization,

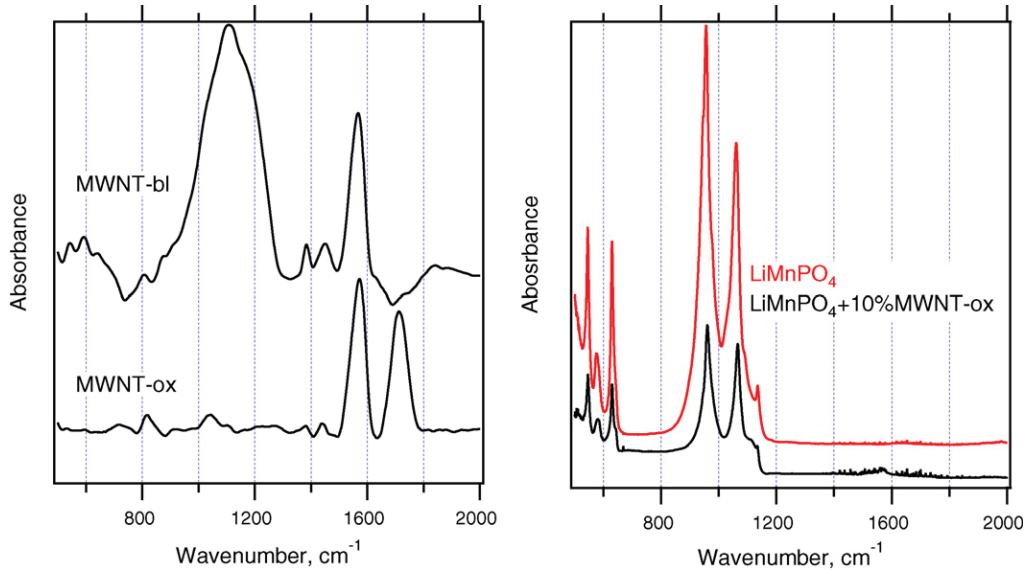


Fig. 4. Left panel: FTIR spectra in KBr pellets of non-functionalized and functionalized nanotubes, MWNT-bl and MWNT-ox, respectively. Right panel: ATR-FTIR spectra of powder of pure $LiMnPO_4$ and $LiMnPO_4$ in a composite with 10 wt% of functionalized nanotubes MWNT-ox. Spectra are offset for clarity.

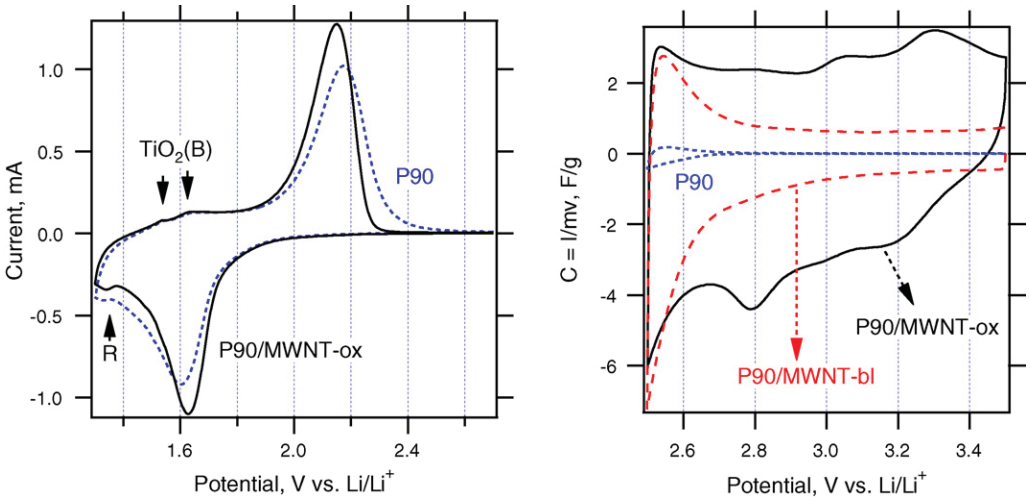


Fig. 5. Cyclic voltammograms of titanium dioxide (P90) thin film electrodes. Full black curves: P90 in a composite with 10 wt% of functionalized nanotubes (P90/MWNT-ox). Dashed blue curve: pure P90. Dashed red curve (right chart only): P90 in a composite with 10 wt% of non- functionalized nanotubes (P90/MWNT-bl). Scan rate 2 mV s^{-1} (left chart) or 50 mV s^{-1} (right chart). The voltammetric features assigned to rutile (R) and TiO_2(B) are marked by arrows. In the right chart, the current is divided by the mass of electrode material and by the scan rate.

there is no conclusive evidence from the IR spectra for this change. First, the skeletal vibration at 1570 cm^{-1} remains intact for both samples and, secondly, the good electrochemical performance of MWNT-ox (see also below) speaks for unperturbed graphitic structure, maintaining high electrical conductivity of nanotubes.

Fig. 4 (right panel) shows ATR-FTIR spectra of the composite $LiMnPO_4$ with 10 wt% MWNT-ox. Also shown is the spectrum of parent pure $LiMnPO_4$. Both spectra are dominated by vibrational features of the PO_4^{3-} group, *viz.* symmetric and antisymmetric bending modes (500–650 cm^{-1}) as well as stretching modes (950–1150 cm^{-1}). These bands remain intact by the interaction with MWNT-ox. The latter component manifests itself by very weak ATR-FTIR features between 1500 and 1800 cm^{-1}, which are assignable to surface oxides including carboxylic groups [50]. These vibration bands are more clearly distinguishable by measurement of MWNT-ox in KBr pellets (left panel, Fig. 4). The vibrational pattern for composites with $LiFePO_4$ is similar (data not shown). Our results are in accord with those for $LiFePO_4$/SWNT/Ru-bipyridine complex, where no shifts of olivine-related vibrations were found upon interaction with nanotubes [47].

Fig. 5 shows the cyclic voltammogram of pure P90 and the composites with nanotubes, P90/MWNT-ox and P90/MWNT-bl. To present comparable data, all electrodes contained similar amounts of TiO_2, around 0.33 mg cm^{-2}. The cyclic voltammograms in the left chart are dominated by a pair of peaks with the formal potential of 1.85 V vs. Li/Li^+, assignable to Li insertion into anatase [18,19,21,22]:

$$x(Li^+ + e^-) + TiO_2 \rightarrow Li_xTiO_2; \quad x \approx 0.5 \tag{3}$$

The total Li-insertion capacity of TiO_2 was determined from the slow scan (0.1 mV s^{-1}) to be 169 or 172 mAh g^{-1} for the P90 or P90/MWNT-ox, respectively. Hence, within the experimental errors, the Li-storage capacities of both materials are identical. This matches the conclusion of most other works on anatase/MWNT composites [14,16,17], although there are also opposite claims for the capacity enhancement in anatase [15]. The beneficial effect of nanotube networking is demonstrated by the shape of cyclic voltammograms of Li-insertion (left chart, Fig. 5): The peak-to-peak separation gets smaller in the composite, and the slopes of insertion onset (around 1.8 V at the cathodic branch) and extraction offset (around 2.2 V at the anodic branch) are steeper for the composite. Particularly, the tail at anodic branch between 2.2 and 2.5 V demonstrates, that extraction of the last portions of the (e^-/Li^+) pairs requires higher overpotential, because the host structure itself (TiO_2) is poorly conducting at these conditions (potentials).

Another important information, which follows from the Li-insertion electrochemistry (Fig. 5, left chart) regards the phase composition of our P90 material. The cathodic peak at 1.35 V is assignable to rutile [18,20,26], which is the expected component of P90 material (see Section 2). Somewhat surprisingly, we also detect tiny amount of monoclinic TiO_2(B) modification of titania. This phase manifests itself by two anodic peaks at 1.55 and 1.65 V, which are diagnostic for the TiO_2(B) phase [25]. It should be noted that the electrochemical Li-insertion is predominantly suitable and highly sensitive method of phase analysis; alternative techniques, viz. X-ray diffraction and Raman spectroscopy did not reveal any TiO_2(B) in our P90 material (data not shown).

Fig. 5 (right chart) shows the details of cyclic voltammogram of our TiO_2–MWNT-ox system in the potential window near the onset of Li-storage in TiO_2. The electrochemical window between 2.5 and 3.5 V is suitable for detailed investigation of pseudocapacitive effects in the composite. Pure TiO_2 expectedly shows no activity, because this potential window is well above the flatband potential, and titania is regarded an insulator in this electrochemical window. The composite TiO_2/MWNT-bl exhibits roughly the capacitive double-layer charging at potentials >ca. 2.8 V, as in pristine MWNT-bl (cf. Fig. 1 and discussion thereof). Because titania is here electrochemically silent, and the concentration of MWNT-bl in the composite was 10 wt%, the found specific capacitance of the composite (≈1 F g^{-1}, cf. Fig. 5, right chart), is assignable solely to that of MWNT-bl.

However, qualitatively new features are observed in the composite TiO_2/MWNT-ox (full curve in Fig. 5, right chart). In contrast to pure MWNT-ox which exhibits just one pair of pseudocapacitive peaks at the formal potential of ca. 3.1 V (Fig. 1), we observe complex pseudocapacitive features in the TiO_2/MWNT-ox composite (Fig. 5, right chart, full curve). A detailed assignment of these peaks cannot be made at this stage, but it is obvious that the interactions between the oxidized (carboxylated) surface of carbon nanotubes and TiO_2 creates new sites for pseudocapacitive interfacial redox chemistry. This matches the conclusion of Reddy and Ramaprabhu [44], but in contrast to this work, we do not observe the dramatic increase of specific capacitance for the composite. The cited authors [44] reported 67 and 160 F g^{-1} for MWNT and TiO_2/MWNT, respectively [44] in aqueous electrolyte solution. Similarly, there was a strong capacitance enhancement in the MWNT composite with

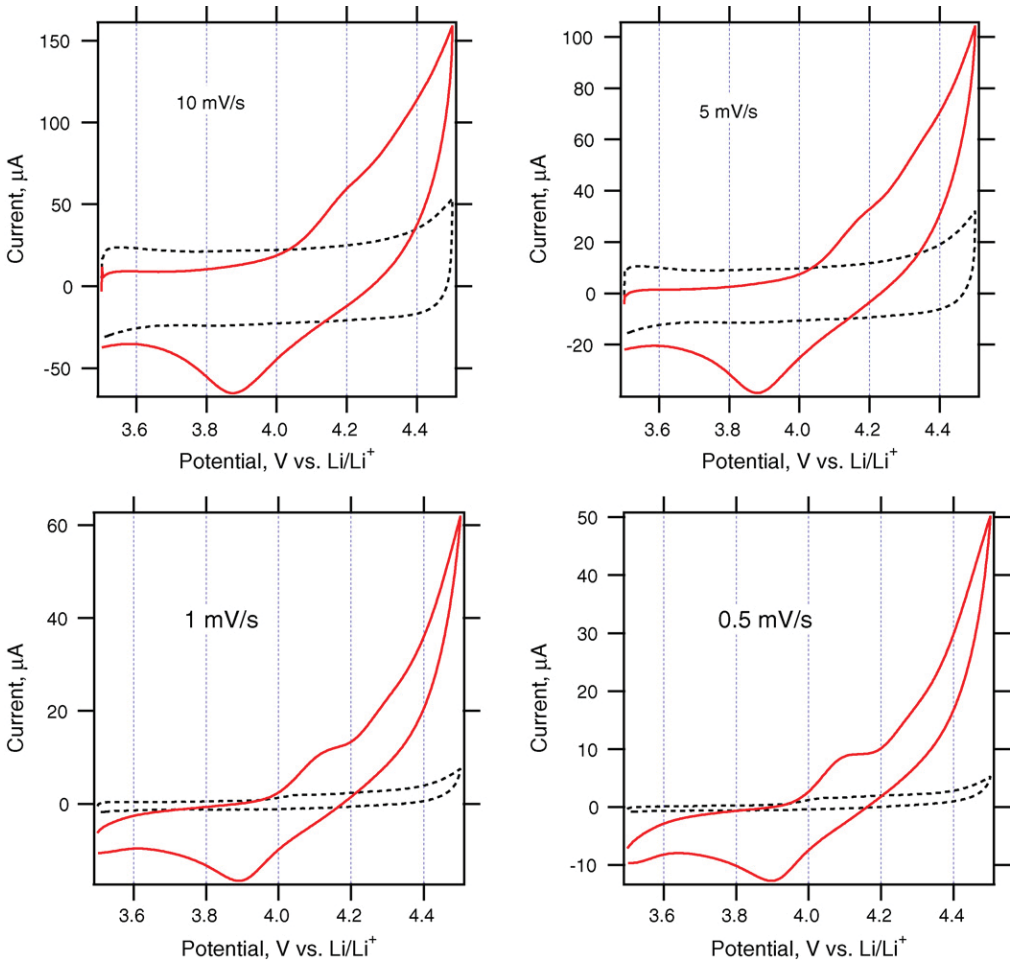


Fig. 6. Cyclic voltammograms of thin film electrodes from $LiMnPO_4$ in a composite with 10 wt% of MWNT-ox (film mass 0.87 mg cm^{-2}; red full curves). The voltammograms of electrodes from pure MWNT-ox are displayed as dashed back curves (film mass 0.20 mg cm^{-2}; these curves are normalized by a factor of 0.435, see text). Scan rates from 10 to 0.5 mV s^{-1} as indicated on each chart.

RuO_2, which is one of the most important oxides for supercapacitors [59]. This was interpreted as coupling of the nanotube-located redox processes (cf. Eq. (2)) with those in protonated ruthenium dioxide:

$$RuO_x(OH)_y + \delta H^+ + \delta e^- \rightarrow RuO_{x-\delta}(OH)_{y+\delta} \quad (4)$$

In our study, employing aprotic Li-containing electrolyte solution, the capacitances are roughly identical (cf. Figs. 1 and 5). Obviously, pseudocapacitive reactions requiring protons are not possible in our electrolyte solution.

Fig. 6 shows a series of cyclic voltammograms of $LiMnPO_4$/MWNT-ox composite (10 wt% MWNT-ox, film mass 0.87 mg cm^{-2}). Also shown are the voltammograms of pure MWNT-ox (the film mass 0.20 mg cm^{-2}; dashed curves in Fig. 6). The latter exhibits just capacitive double-layer charging (cf. Fig. 1). In order to show comparable plots in Fig. 6, the currents for pure MWNT-ox are normalized by a factor of 0.435, which puts the amount of MWNT-ox in both electrodes to identical values. At faster scan rates, we can trace similar voltammetric charge assignable to pure double-layer charging in the composite electrode at potentials around 3.6 V, where no significant faradaic processes in $LiMnPO_4/MnPO_4$ are expected. The latter are found near the formal potential of 4.1 V, which is the Nernstian potential of this reaction [27,33,34]:

$$LiMnPO_4 \leftrightarrow MnPO_4 + Li^+ + e^- \quad (5)$$

The integral cathodic voltammetric charge at the slow scan rate (0.1 mV s^{-1}; data not shown) translates into the reversible charge capacity of 13 mAh g^{-1} at the cut-off voltage of 3.5 V. (The anodic scan provides larger values, which are not representative, because of electrolyte decomposition, see Fig. 6). If we extend the lower cut-off voltage to 3 V, the same electrode provides reversible capacity of 24 mAh g^{-1}. These values are roughly comparable to those of $LiMnPO_4$/MWNT composite reported by Manthiram et al. [32]. They used galvanostatic discharge of an electrode containing 8% of MWNT in $LiMnPO_4$, but their electrodes further contained massive amounts of carbonaceous additives, *viz.* 25 wt% of conductive carbon (of unknown origin) and 25% of teflonized acetylene black [32]. Therefore, their blank electrodes, fabricated from a MWNT-free material, did exhibit discharge capacities of ca. 25–30 mAh g^{-1} (depending on the discharge current) at the cut-off voltage of 2 V, and these values slightly increased to ca. 35–45 mAh g^{-1} for the MWNT-containing material [32].

In our case, the activation of $LiMnPO_4$ by nanotubes is demonstrated on a simpler system, omitting all other carbonaceous additives except MWNT. Fig. 7 confirms that the capacity of pure $LiMnPO_4$ is negligible due to its very low conductivity. Also the beneficial effect of surface oxidation is demonstrated by comparing the composites containing MWNT-bl and MWNT-ox. Here we show the data for nanotube/$LiMnPO_4$ electrodes of roughly comparable film masses around 0.85 mg cm^{-2}. The peak current for anodic process in olivine, that is oxidation of $LiMnPO_4$ to $MnPO_4$ (Eq. (5)) is roughly identical for both electrodes, but the material

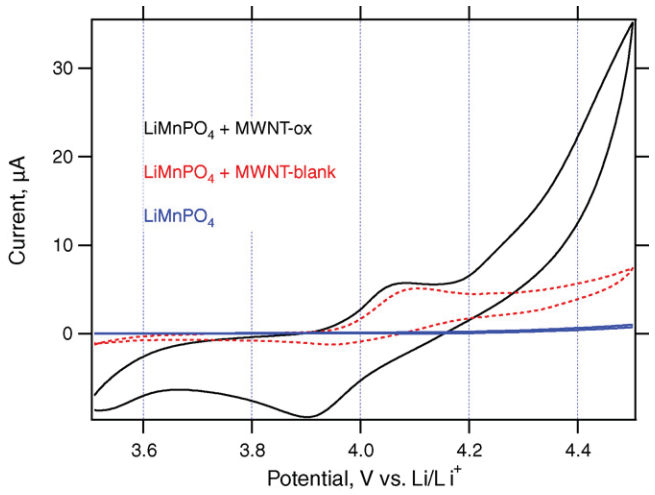


Fig. 7. Cyclic voltammograms of $LiMnPO_4$ thin film electrodes in a composite with 10 wt% of MWNT-ox (film mass 0.83 mg cm^{-2}). Red dashed curve: $LiMnPO_4$ in a composite with 10 wt% of MWNT-bl, film mass 0.87 mg cm^{-2}; the same film like in Fig. 6). Blue curve: pure $LiMnPO_4$ (film mass 1.05 mg cm^{-2}) Scan rate 0.2 mV s^{-1}.

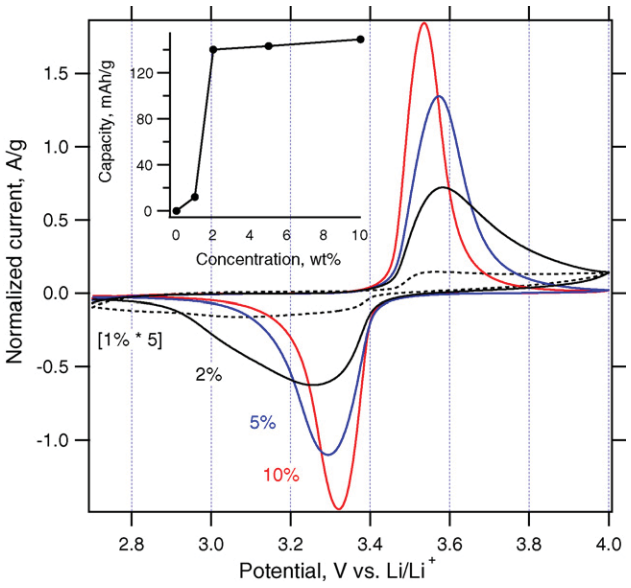


Fig. 9. Cyclic voltammograms of $LiFePO_4$ in a composite with functionalized nanotubes, MWNT-ox. The concentration of MWNT-ox in the composite varied between 1 and 10 wt%. Currents are normalized to the actual mass of $LiFePO_4$ in the thin-film electrode, and for the voltammogram of 1 wt% composite, the current was zoomed by a factor of 5. Scan rate 0.5 mV s^{-1}. Inset shows the integral voltammetric charge capacity as a function of the concentration of MWNT-ox in the composite.

with MWNT-bl shows very small cathodic charge for the reverse reaction. Hence the oxidative treatment of nanotubes improves the reversibility of $LiMnPO_4$ charge/discharge. However, the surface oxidation of nanotubes also activates the electrolyte decomposition. This is demonstrated by anodic branch of our voltammograms between 4.2 and 4.5 V. The surface oxides (carboxyls) mediate these parasitic breakdown reactions, although the mechanism of this activation is unknown. (Note that enhanced breakdown of electrolyte solution is traceable also on pure MWNT-ox film shown in Fig. 1 above.)

In contrast to $LiMnPO_4$ where the electrochemical activation by nanotubes is quite weak, the $LiFePO_4$ olivine exhibits excellent performance in a composite with MWNT-ox. Fig. 8 shows cyclic voltammograms similar to those presented in Fig. 7 for $LiMnPO_4$. The improvement caused by surface oxidation of nanotubes is dramatic. The composite $LiFePO_4$/MWNT-ox exhibits a capacity of 149 mAh g^{-1} (at the scan rate of 0.1 mV s^{-1}) and nearly perfect charge/discharge reversibility of 99–100%. These impressive values were independent on the film mass in the whole tested array of samples, up to ca. 1 mg cm^{-2}. On the other hand, the $LiFePO_4$/MWNT-bl attains only 32 mAh g^{-1} at the same conditions (cf. Fig. 8) although the charging reversibility is again close to 100%.

Obviously, the electrolyte breakdown reactions are unimportant for this system, that is charging up to the upper vertex potential of 4 V only, and the charge reversibility is perfect.

This promising system has been subjected to further optimization. Fig. 9 shows cyclic voltammograms for a series of composite materials $LiFePO_4$/MWNT-ox, in which the concentration of MWNT-ox varied. Perfect charge reversibility is again maintained for all materials, but there is a sudden drop of charge capacity for MWNT-ox concentrations between 1 and 2 wt% (see Fig. 9, inset). This seems to be the effective charge-percolation threshold in our composite. Fig. 10 (left chart) further documents this finding by additional performance tests at varying scan rates. The materials with 2–10% MWNT-ox behave roughly similarly, although the performance improves expectedly with increasing concentration. Fig. 10 (right chart) also compares the Li-storage capacity of composite materials with various degrees of nanotube oxidation, that is (in concentrations of acidic groups): 2.54×10^{-4} mol g^{-1}

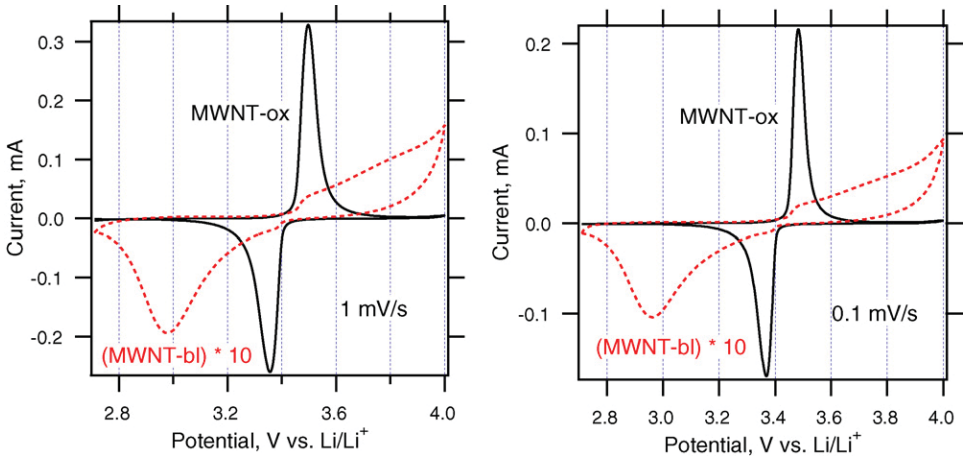


Fig. 8. Cyclic voltammograms of $LiFePO_4$ thin film electrodes. Black full curve: $LiFePO_4$ in a composite with 10 wt% of functionalized nanotubes, MWNT-ox (film mass 0.33 mg cm^{-2}). Red dashed curve: $LiFePO_4$ in a composite with 10 wt% of non-functionalized MWNT-bl (film mass 0.38 mg cm^{-2}); this curve is zoomed by a factor of 10 in the current scale. Scan rate 1 or 0.1 mV s^{-1} for the left or right charts, respectively.

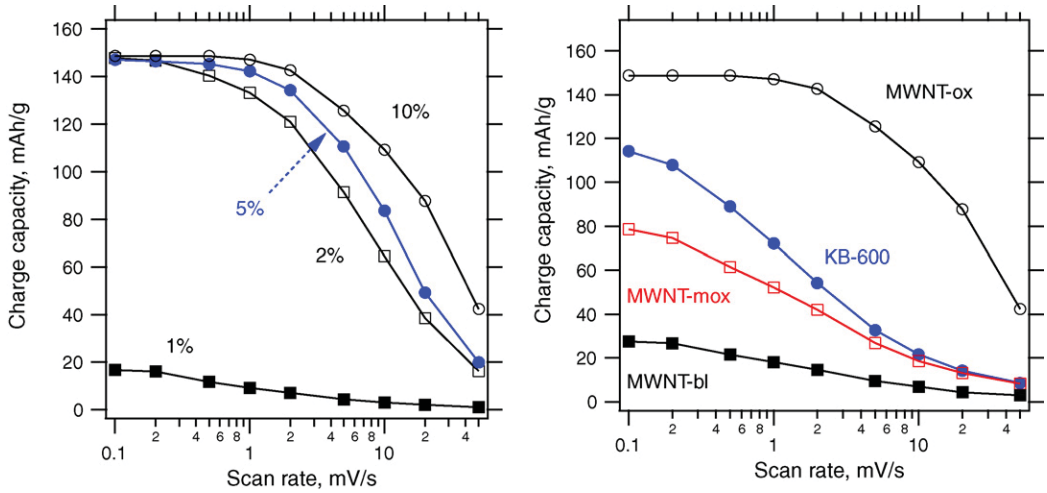


Fig. 10. Integral voltammetric charge capacity as a function of scan rate. (Left chart): $LiFePO_4$ in a composite with functionalized nanotubes, MWNT-ox. The concentration of MWNT-ox in the composite varied between 1 and 10 wt% (as in Fig. 9). (Right chart): $LiFePO_4$ in a composite with the following carbonaceous materials: oxidized nanotubes (MWNT-ox; 2.54×10^{-4} mol g^{-1} acidic groups), medium-functionalized nanotubes (MWNT-mox; 1.14×10^{-4} mol g^{-1} acidic groups), non-functionalized nanotubes (MWNT-bl) and carbon black KB-600. The concentration was 10 wt% in all composites shown in the left chart.

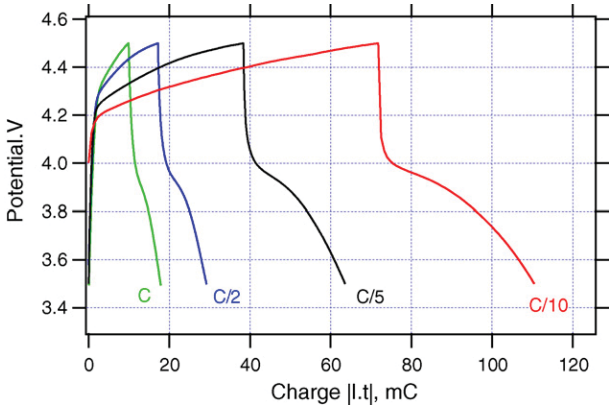


Fig. 11. Galvanostatic chronopotentiometry of $LiMnPO_4$ in a composite with 10 wt% of functionalized nanotubes, MWNT-ox (film mass 0.62 mg cm^{-2}). Discharge/charge cycles are shown for varying charge rates from C/10 to C.

(MWNT-ox); 1.14×10^{-4} mol g^{-1} (MWNT-mox) and ≈0 (MWNT-bl). Somewhat surprisingly, the composite containing MWNT-bl is even less efficient than the composite made from ordinary commercial carbon black, KB-600. It is obvious that the functionalization of nanotubes is, indeed, crucial for enhancing the electrochemical activity of the composite materials with $LiFePO_4$.

The conclusions from cyclic voltammetry are further supported by discharge/charge cycles which were tested using galvanostatic chronopotentiometry. Fig. 11 shows the initial discharge/charge of $LiMnPO_4$/MWNT-ox at varying charge rates from C/10 to C. A similar plot for $LiFePO_4$/MWNT-ox is shown in Fig. 12. While the first system exhibits poor performance with considerable irreversibility, the latter is good. The particular electrode shown in Fig. 12 has the theoretical charge capacity of 353 mC (170 mA g^{-1}), while 88% of this capacity can be reversibly cycled at C/2. This electrode can still deliver 38% of its theoretical capacity at 50C, that is within 72 s (Fig. 12). It is interesting to note that the charge capacity observed at C/2, C, 5C, 10C, etc., is roughly similar to the voltammetric charge capacity at scan rates (in mV s^{-1}) of 0.5, 1, 5, 10, etc.

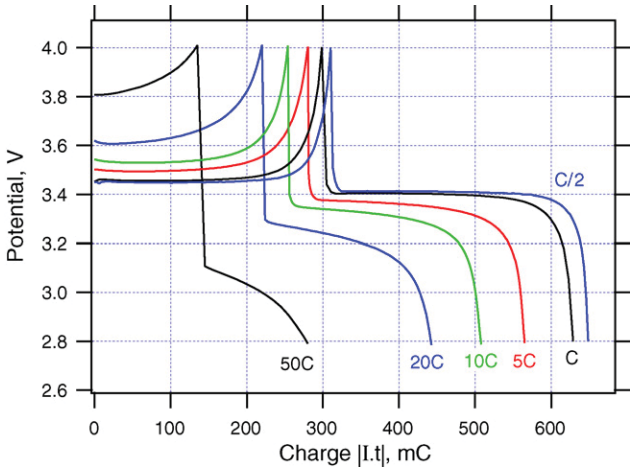


Fig. 12. Galvanostatic chronopotentiometry of $LiFePO_4$ in a composite with 10 wt% of functionalized nanotubes, MWNT-ox (film mass 0.68 mg cm^{-2}). Discharge/charge cycles are shown for varying charge rates from C/2 to 50C.

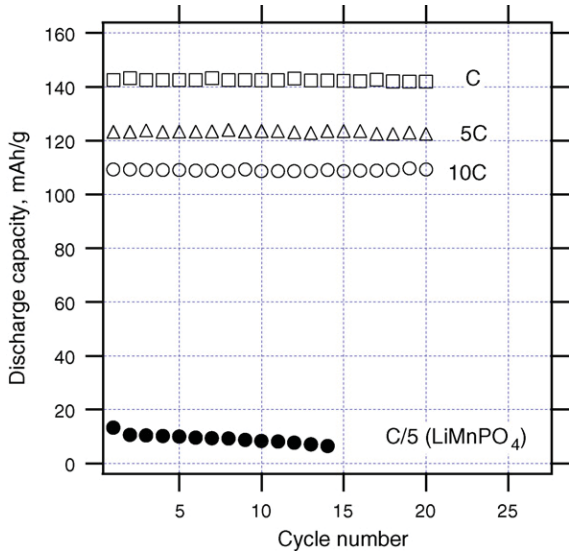


Fig. 13. Discharge capacity determined from galvanostatic chronopotentiometry (as in Figs. 11 and 12) for several successive discharge/charge cycles. The top three curves are for $LiFePO_4$ in a composite with 10 wt% of functionalized nanotubes, MWNT-ox (film mass 0.68 mg cm^{-2}); the charge/discharge rates were: C (squares), 5C (triangles) and 10C (open points). The bottom curve is for $LiMnPO_4$ in a composite with 10 wt% of functionalized nanotubes, MWNT-ox (film mass 0.62 mg cm^{-2}); the charge/discharge rate was C/5 (full points).

(cf. Fig. 10). Obviously, both experiments require comparable times for completing the discharge/charge, and they give similar charge capacities. Fig. 13 shows that the electrode $LiMnPO_4$/MWNT-ox loses ca. half of its initial capacity during 15 subsequent discharge/charge cycles at C/5. This illustrates the conclusions from chronopotentiometry (Fig. 11) and voltammetry (Figs. 6 and 7) that the process is irreversible due to anodic electrolyte breakdown enhanced by MWNT-ox. On the other hand, the cycle life of $LiFePO_4$/MWNT-ox is excellent: we do not see any breakdown during twenty cycles which were repeatedly carried out for the same electrode at C, 5C and 10C (Fig. 13). In subsequent experiments (data not shown) our electrode survived hundreds of cycles without marked decomposition, which would cause any loss of its charge capacity.

4. Conclusions

A comparative study was carried out to investigate composite materials in which multi-walled carbon nanotubes, either pristine or functionalized by carboxyls, were interfaced to three different materials, viz. TiO_2, $LiMnPO_4$ and $LiFePO_4$. The functionalization of nanotubes was followed by FTIR, and by titration analysis of the acidic groups. At comparable conditions, specific features of each combination of materials in the composites are highlighted by electrochemistry in Li-containing aprotic medium.

Functionalized multi-walled carbon nanotubes exhibit improved affinity towards TiO_2. This was demonstrated using industrial powder P90 from Degussa, which is anatase-rutile mixture (>90% anatase) with small amount of TiO_2(B). The latter phase is detectable only by highly sensitive electrochemical analysis shown here. The Li-storage capacity of TiO_2 is not enhanced in the composite, but the rate of electrochemical charge transfer is higher due to nanotube networking. Complex pseudocapacitive features are observed at potentials near the onset of Li-storage in pure anatase. Whereas the composite with pristine nanotubes shows just simple superposition of the behavior of pure components, that is TiO_2 and MWNT-bl (with dominating double-layer capacitive response of pristine MWNT-bl), the composite with functionalized nanotubes shows unique faradaic pseudocapacitance, which is specific only for the interaction of functionalized MWNT-ox with the titania surface.

The composite of $LiMnPO_4$ (olivine) with functionalized multi-walled carbon nanotubes shows enhanced electrochemical charge/discharge performance, which, however, is not comparable to that of the state-of-art carbon-coated $LiMnPO_4$ (olivine). The beneficial effect of surface functionalization consists in improved charge storage capacity and improved charging/discharging reversibility. However, the surface functionalization also promotes the electrolyte breakdown at potentials >4.2 V, which are near the operational conditions of this cathode material in Li-ion batteries.

In contrast to $LiMnPO_4$, excellent electrochemical activation of $LiFePO_4$ by functionalized nanotubes was found. The charging was reversible near 100% and was unperturbed during repeated discharge/charge cycling. This confirms that there was no significant nanotube-mediated electrolyte breakdown at the operating voltage of $LiFePO_4$ (olivine) cathode in Li-ion batteries. Composite material containing only 2 wt% of MWNT-ox showed nearly the nominal charge capacity at the time-scale of cyclic voltammetry, scan rates <0.2 mV s^{-1}. The percolation threshold for nanotube networking of our $LiFePO_4$ was between 1 and 2 wt% of MWNT-ox in the composite. The functionalization of nanotubes via surface oxidation is crucial for the activation of $LiFePO_4$. The composite with pristine nanotubes showed rather low activity, which is even smaller than that of the composite with high surface area carbon black.

Acknowledgements

This work was supported by the Swiss National Science Foundation, Czech Ministry of Education, Youth and Sports (contract No. LC-510 and OC09048), the COST Action D35, and by the Academy of Sciences of the Czech Republic (contract IAA 400400804, KAN200100801 and KAN100500652). We are grateful to HPL, SA for providing us with olivine samples.

References

[1] X. Peng, J. Chen, J.A. Misewich, S.S. Wong, Chem. Soc. Rev. 38 (2009) 1076–1098.
[2] B. Liu, C. Zeng, Chem. Mater. 20 (2008) 2711–2718.
[3] G. An, W. Ma, Z. Sun, Z. Liu, B. Han, S. Miao, Z. Miao, K. Ding, Carbon 45 (2007) 1795–1801.
[4] B. Gao, Z.C. Chen, G.L. Puma, Appl. Catal. B 89 (2009) 503–509.
[5] L.C. Chen, Y.C. Ho, W.S. Guo, C.M. Huang, T.C. Pan, Electrochim. Acta 54 (2009) 3884–3891.
[6] H. Wang, H.L. Wang, W.F. Jiang, Chemosphere 75 (2009) 1105–1111.
[7] K. Dai, T. Peng, D. Ke, B. Wei, Nanotechnology 20 (2009) 125603–1256036.
[8] C.Y. Yen, Y.F. Lin, S.H. Liao, C.C. Weng, C.C. Huang, Y.H. Hsiao, C.C.M. Ma, M.C. Chang, H. Shao, M.C. Tsai, C.K. Hsieh, C.H. Tsai, F.B. Weng, Nanotechnology 19 (2008) 375305–3753059.
[9] T.Y. Lee, P.S. Alegaonkar, J.B. Yoo, Thin Solid Films 515 (2007) 5131–5135.
[10] S.L. Kim, S.R. Jang, R. Vittal, J. Lee, K.J. Kim, J. Appl. Electrochem. 36 (2006) 1433–1439.
[11] T. Sawatsuk, A. Chindaduang, S.K. Chaiyuth, S. Pratontep, G. Tumcharen, Diamond Rel. Mater. 18 (2009) 524–527.
[12] A. Kongkanand, R.M. Dominguez, P.V. Kamat, Nano Lett 7 (2007) 676–680.
[13] D.H. Lee, J.G. Park, K.J. Choi, H.J. Choi, D.W. Kim, Eur. J. Inorg. Chem. 2008 (2008) 878–882.
[14] O. Frank, M. Kalbac, L. Kavan, M. Zukalova, J. Prochazka, M. Klementova, L. Dunsch, Phys. Stat. Sol. (b) 244 (2007) 4040–4045.
[15] J. Li, S. Tang, L. Lu, C. Zeng, J. Am. Chem. Soc. 129 (2007) 9401–9409.
[16] I. Moriguchi, Y. Shono, H. Yamada, T. Kudo, J. Phys. Chem. B 112 (2008) 14560–14565.
[17] H. Huang, W.K. Zgang, X.P. Gan, C. Wamg, L. Zhang, Mater. Lett. 61 (2007) 296–299.
[18] L. Kavan, Adv. Sci. Technol. 51 (2006) 20–29.
[19] M. Wagemaker, W.J.H. Borghols, F.M. Mulder, J. Am. Chem. Soc. 129 (2007) 4323–4327.
[20] D. Wang, D. Choi, V.V. Viswanathan, Z. Nie, C. Wang, Y. Song, J.G. Zhang, J. Liu, Chem. Mater. 20 (2008) 3435–3442.
[21] S.Y. Huang, L. Kavan, M. Grätzel, I. Exnar, J. Electrochem. Soc. 142 (1995) 142–144.
[22] I. Exnar, L. Kavan, S.Y. Huang, M. Grätzel, J. Power Sources 68 (1997) 720–722.
[23] A.R. Armstrong, G. Armstrong, J. Canales, P.G. Bruce, Angew. Chem. Int. Ed. 43 (2004) 2286–2288.
[24] A.R. Armstrong, G. Armstrong, J. Canales, R. Garcia, P.G. Bruce, Adv. Mater. 17 (2005) 862–865.
[25] M. Zukalova, M. Kalbac, L. Kavan, I. Exnar, M. Grätzel, Chem. Mater. 17 (2005) 1248–1255.
[26] N.A. Milne, M.S. Kazacos, V. Luca, J. Phys. Chem. C 113 (2009), 12995-.
[27] A.K. Padhi, K.S. Nanjundasawamy, J.B. Goodenough, J. Electrochem. Soc. 144 (1997) 1188–1194.
[28] B. Ellis, L.K. Perry, D.H. Ryan, L.F. Nazar, J. Am. Chem. Soc. 128 (2006).
[29] S.Y. Chung, J.T. Bloking, Y.M. Chiang, Nat. Mater. 1 (2002) 123–128.
[30] P.S. Herle, B. Ellis, N. Coombs, L.F. Nazar, Nat. Mater. 3 (2004) 147–152.
[31] N. Meetlong, H.Y.J.S. Huang, S.A. Speakman, W.C. Carter, Y.M. Chiang, Adv. Funct. Mater. 17 (2007) 1115–1123.
[32] A.V. Murugan, T. Muraliganth, P.J. Ferreira, A. Manthiram, Inorg. Chem. 48 (2009) 946–952.
[33] D. Wang, H. Buqa, M. Crouzet, G. Deghenghi, T. Drezen, I. Exnar, N.H. Kwon, J. Miners, L. Poletto, M. Grätzel, J. Power Sources 189 (2009) 624–628.
[34] S.K. Martha, B. Markovsky, J. Grinblat, Y. Gofer, O. Haik, E. Zinigrad, D. Aurbach, T. Drezen, D. Wang, G. Deghenghi, I. Exnar, J. Electrochem. Soc. 156 (2009) A541–A552.
[35] B. Jin, H.B. Gu, W. Zhang, K.H. Park, G. Sun, J. Solid State Electrochem. 12 (2008) 1549–1554.
[36] Y. Liu, X. Li, H. Guo, Z. Wang, W. Peng, Y. Yang, R. Liang, J. Power Sources 184 (2008) 522–526.
[37] X. Li, F. Kang, X. Bai, W. Shen, Electrochem. Commun. 9 (2007) 663–666.
[38] J.C. Chen, M.S. Whittingham, Electrochem. Commun. 8 (2006) 855–858.
[39] M.M. Doeff, J.D. Wilcox, R. Yu, A. Aumentado, M. Marcinek, R. Kostecki, J. Solid State Electrochem. 12 (2008) 995–1001.
[40] L. Wang, Y. Huang, R. Jiang, D. Jia, J. Electrochem. Soc. 154 (2007) A1015–A1019.
[41] T. Muraliganth, A.V. Murugan, A. Manthiram, J. Mater. Chem. 18 (2008) 5661–5668.
[42] B. Jin, K.H. Park, H.B. Gu, Electrochem. Commun. 10 (2008) 1537–1540.
[43] Y.J. Lee, H. Yi, W.J. Kim, K. Kang, D.S. Yun, M.S. Strano, G. Ceder, A.M. Belcher, Science 324 (2009) 1051–1055.
[44] A.L.M. Reddy, S. Ramaprabhu, J. Phys. Chem. C 111 (2007) 7727–7734.
[45] L. Kavan, I. Exnar, J. Cech, M. Grätzel, Chem. Mater. 19 (2007) 4716–4721.

[46] L. Kavan, I. Exnar, S.M. Zakeeruddin, M. Grätzel, J. Phys. Chem. C 112 (2008) 8708–8714.
[47] L. Kavan, S.M. Zakeeruddin, I. Exnar, M. Grätzel, J. Electrochem. Soc. 156 (2009) K44–K50.
[48] L. Kavan, O. Frank, M. Kalbac, L. Dunsch, J. Phys. Chem. C 113 (2009) 2611–2617.
[49] M. Corrias, B. Caussat, A. Ayral, J. Durand, Y. Kihn, P. Kalck, P. Serp, Chem. Eng. Sci. 58 (2003) 4475–4482.
[50] A. Solhy, B.F. Machado, J. Beausoleil, Y. Kihn, F. Goncalves, M.F.R. Pereira, J.J.M. Orfao, J.L. Figueiredo, J.L. Faria, P. Serp, Carbon 46 (2009) 1194–1207.
[51] E. Frackowiak, K. Metenier, V. Bertagna, F. Beguin, Appl. Phys. Lett. 77 (2000) 2421–2423.
[52] C. Li, D. Wang, X. Wang, J. Liang, Carbon 43 (2005) 1557–1583.
[53] E. Frackowiak, S. Gautier, H. Gaucher, S. Bonnamy, F. Béguin, Carbon 37 (1999) 61–69.
[54] E. Frackowiak, F. Béguin, Carbon 40 (2002) 1775–1787.
[55] C.C. Hu, J.H. Su, T.C. Wen, J. Phys. Chem. Solids 68 (2007) 2353–2362.
[56] Y.T. Kim, Y. Ito, K. Tadai, T. Mitani, U.S. Kim, H.S. Kim, B.W. Cho, Appl. Phys. Lett. 87 (2005) 234106–2341063.
[57] J.T. Kloprogge, R.L. Frost, Thermochim. Acta 320 (1998) 245–252.
[58] T.G. Ros, A.J. van Dillen, J.W. Geus, D.C. Konigsberger, Chem. Eur. J. 8 (2002) 1151–1162.
[59] G. Arabal, D. Wang, M. Kulkarni, I.S. Mulla, S.P. Vernekar, K. Vijayamohanan, A.M. Rao, Chem. Phys. Lett. 376 (2003) 207–213.

APPENDIX KAVAN03

https://www.sciencedirect.com/science/article/abs/pii/S0378775310004180 June 6, 2024

ScienceDirect Journals & Books Help Search My account Sign in

Access through your institution Purchase PDF

Article preview

Abstract

Introduction

Section snippets

References (59)

Cited by (74)

Journal of Power Sources

Volume 195, Issue 16, 15 August 2010, Pages 5360-5369

Multi-walled carbon nanotubes functionalized by carboxylic groups: Activation of TiO_2 (anatase) and phosphate olivines ($LiMnPO_4$; $LiFePO_4$) for electrochemical Li-storage

Ladislav Kavan [a], Revathi Bacsa [b], Meltem Tunckol [b], Philippe Serp [b], Shaik M. Zakeeruddin [c], Florian Le Formal [c], Marketa Zukalova [a], Michael Graetzel [c]

[a] J. Heyrovský Institute of Physical Chemistry, v.v.i., Academy of Sciences of the Czech Republic, Dolejškova 3, CZ-18223 Prague 8, Czech Republic

[b] Laboratoire de Chimie de Coordination, UPR CNRS 8241, composante ENSIACET, Université de Toulouse UPS-INP-LCC 4, Allée Emile Monso, BP 74233, 31432, Toulouse, France

[c] Laboratoire de Photonique et Interfaces, EPFL, Ecublens, CH-1015 Lausanne, Switzerland

Received 18 November 2009, Revised 9 February 2010, Accepted 6 March 2010, Available online 12 March 2010.

What do these dates mean?

Show less

+ Add to Mendeley Share Cite

https://doi.org/10.1016/j.jpowsour.2010.03.028 Get rights and content

Abstract

Multi-walled carbon nanotubes functionalized by carboxylic groups, exhibit better affinity towards TiO_2 (P90, Degussa) as compared to that of pristine nanotubes. Also the electrochemical performance of TiO_2 is improved by nanotube networking, but the Li-storage capacity of TiO_2 is unchanged. Whereas the composite of TiO_2 with non-functionalized nanotubes demonstrates simple superposition of the behavior of pure components, the composite with functionalized nanotubes shows unique faradaic pseudocapacitance which is specific for this composite only. The surface functionalization of nanotubes enhances charge storage capacity and reversibility of a composite with $LiMnPO_4$ (olivine), but mediates also the electrolyte breakdown at potentials >4.2V. Whereas the electrochemical activation of $LiMnPO_4$ (olivine) by functionalized nanotubes is quite modest, excellent performance was found for $LiFePO_4$ (olivine) in composite materials containing only 2wt% of functionalized nanotubes.

Introduction

Carbon nanotubes form conductive composites with inorganic nanocrystals (for recent review see Ref. [1]). Compared to single-wall carbon nanotubes (SWNT) the multi-walled carbon nanotubes (MWNT) are cheaper, mechanically more robust and their electrical conductivity is less affected by

Recommended articles

The effects of retinoic acid on mmp-2 production, proliferation and...
Experimental and Toxicologic Pathology, Volu...
Tuğba Kotil, ..., Leyla Tapul

Predominant electronic conductivity of $Li_2ZnTi_3O_8$ anode material prepar...
Journal of Electroanalytical Chemistry, Volume ...
Haoqing Tang, ..., Zhiyuan Tang

Nicotinic receptors modulate the function of presynaptic AMPA...
Neurochemistry International, Volume 90, 2015...
Irene A. Samengo, ..., Maria Martire

Show 3 more articles

Article Metrics

Citations

Citation Indexes: 74

Captures

Readers: 70

PLUMX View details

chemical functionalization. Composite materials of MWNT with titanium dioxide have been investigated for application in photocatalysis [2], [3], [4], [5], [6] including photocatalytic hydrogen generation [7] and dye-sensitized solar cells [8], [9], [10], [11]. In these applications, the beneficial role of MWNT is assumed to consist in improved separation of photogenerated charges, but very low MWNT concentrations (<1 wt%) are required to avoid charge recombination with the electrolyte in dye-sensitized solar cells [8], [9], [10], [11]. Improved separation of photogenerated electrons/holes was also demonstrated in solar cells based on band-gap excitation of TiO_2 dispersed on SWNT [12]. The electrochemical lithium storage in carbon nanotube/TiO_2 composites has been studied, too [13], [14], [15], [16], [17], reflecting the fact that TiO_2 (especially anatase [18], [19], [20], [21], [22], TiO_2(B) [18], [23], [24], [25] and rutile [18], [20], [26]) belong to the top interesting host structures for lithium insertion. These studies confirmed in unison that the electrochemical activity of the composite TiO_2/nanotubes is improved compared to that of the parent pure TiO_2 [13], [14], [15], [16], [17]. Some authors reported on significantly enhanced Li-storage capacity of the TiO_2/MWNT nanocomposite [13], [15], but others [14], [16], [17] did not support this observation.

From the viewpoint of electrochemical lithium storage, the phosphate olivines [27], *viz*. $LiMPO_4$ (M=Fe, Mn) have been extensively studied in the past. They are promising cathode materials for Li-ion batteries due to high safety, low cost and environmental tolerability. However, their poor electrical conductivity is a crucial issue to be addressed [28] either by doping [29] or by surface coating with elemental carbon [30], [31]. The conductivity problem is considerably more significant for $LiMnPO_4$ (conductivity of $\approx 10^{-14} Scm^{-1}$ compared to $\approx 10^{-9} Scm^{-1}$ for $LiFePO_4$) [32] but optimization of the synthesis, that is the formation of carbon coating via ball-milling, provided reasonably active materials, too [33], [34].

The effect of MWNT on improvement of the performance of $LiFePO_4$ has been reported by several studies in the past [32], [35], [36], [37], [38], [39], [40], [41], [42]. The synthetic strategies range from simple mixing [32], [36], [37], [40], [41], ball-milling [35], [42], hydrothermal synthesis [38], in situ formation of MWNT from ferrocene [39] up to a bio-inspired route, that is a gene manipulation, which was used to align $LiFePO_4$ with SWNT [43]. An analogous electrochemical activation of $LiMnPO_4$ in a composite with MWNT was reported only recently [32]. In this case, the improvement of charging rate and capacity was quite modest [32], and not comparable to that of the optimized materials, fabricated via ball milling with carbon black [33], [34].

The surface oxidation of carbon nanotubes by HNO_3 [6], [8], [10], [15], [16], [32], [37], [41], [44], H_2SO_4/HNO_3 [4] or H_2O_2 [9], producing among other groups also carboxyls, was sometimes mentioned to improve the anchoring of TiO_2 [4], [6], [8], [9], [10], [15], [16], [44] or $LiMPO_4$ [32], [37], [41]. In the first case, there is a clear analogy with the strong interaction of carboxyl-containing molecules (Ru-bipyridine dyes) with the TiO_2 surface, which is crucial in dye-sensitized solar cells [10]. However, there are also reports that the oxidative functionalization is not necessary for anchoring to TiO_2, because the pristine MWNT behave similarly [15]. The interaction of carboxyls with phosphate olivine surface is less understood, but certainly important, too [45], [46]. To the best of our knowledge, there is no systematic study of these contradictory issues, although detailed understanding is desirable of the MWNT functionalization (by surface oxidation forming carboxyls) for optimum attachment of MWNT towards titania or olivine surfaces.

This was the central motivation for the study reported here. A second argument for deeper investigation of these composites is based on our previous experience with a supramolecular assembly of SWNT with carboxyl-containing Ru–bipyridine complex [45], [46], [47], [48]. This assembly offers unique electrochemical activation of $LiFePO_4$ called 'nanotube wiring' [45], [46]. The advantage of our nanotube wiring consists in the fact, that it keeps the amount of conductive additives in the active electrode material at its natural minimum (≈0.04 wt% of carbon in $LiFePO_4$). This is important for optimization of Li-ion batteries. The reason is that the electrode materials, *viz*. olivines or TiO_2 [21], [22] require *ca*. 10–20 wt% of graphitic carbon to be

added. However, graphite does not contribute to the faradaic reaction in the cathode, but presents ballast, decreasing the charge (energy) density of the composite electrode in the same proportion. Obviously, simple oxidation of MWNT is an attractive and cheap alternative to our 'nanotube wiring' effect [45], [46] for practical Li-ion batteries. Since TiO_2 is a prospective anode material, and $LiMPO_4$ olivines are promising cathode materials, concerted study of the interaction of MWNT with these three selected materials at defined comparable conditions is relevant for the development of high-power Li-ion batteries.

Section snippets

Experimental

Multi-walled carbon nanotubes were prepared from ethylene gas by chemical vapor deposition. The synthesis was carried out in a fluidized bed reactor, and Fe nanoparticles supported on alumina served as catalyst. Details on the reactor configuration and preparation of the catalyst can be found elsewhere [49]. The catalyst was removed by boiling with diluted sulfuric acid (50%) at 140°C for 3h after which the nanotubes were filtered when hot by a glass frit followed by washing with hot water and…

Results and discussion

Fig. 1 shows cyclic voltammogram of thin-film electrode from pure non-functionalized nanotubes, MWNT-bl and the functionalized nanotubes, MWNT-ox. The voltammogram of MWNT-bl confirms an almost ideal double-layer charging in a broad window of electrochemical potentials. Therefore, the voltammetric currents scale with the first power of scan rate, v as it is expected for capacitive charging: $I = \frac{dQ}{dt} = C_{dl} \times \frac{dE}{dt} = C_{dl} v$, Q is the voltammetric charge, $dE/dt = v$ is the scan rate and C_{dl} is the double-layer…

Conclusions

A comparative study was carried out to investigate composite materials in which multi-walled carbon nanotubes, either pristine or functionalized by carboxyls, were interfaced to three different materials, viz. TiO_2, $LiMnPO_4$ and $LiFePO_4$. The functionalization of nanotubes was followed by FTIR, and by titration analysis of the acidic groups. At comparable conditions, specific features of each combination of materials in the composites are highlighted by electrochemistry in Li-containing aprotic…

Acknowledgements

This work was supported by the Swiss National Science Foundation, Czech Ministry of Education, Youth and Sports (contract No. LC-510 and OC09048), the COST Action D35, and by the Academy of Sciences of the Czech Republic (contract IAA 400400804, KAN200100801 and KAN100500652). We are grateful to HPL, SA for providing us with olivine samples….

References (59)

G. An *et al.*
Carbon (2007)

B. Gao *et al.*
Appl. Catal. B (2009)

L.C. Chen *et al.*
Electrochim. Acta (2009)

H. Wang *et al.*

Chemosphere (2009)

T.Y. Lee *et al.*
Thin Solid Films (2007)

T. Sawatsuk *et al.*
Diamond Rel. Mater. (2009)

H. Huang *et al.*
Mater. Lett. (2007)

I. Exnar *et al.*
J. Power Sources (1997)

D. Wang *et al.*
J. Power Sources (2009)

Y. Liu *et al.*
J. Power Sources (2008)

View more references

Cited by (74)

Porous spheres of TiO<inf>2</inf> (B)/anatase entwined by graphene nanoribbons for high Li⁺ rate performance

2019, Electrochimica Acta

> *Citation Excerpt :*
> ...Moreover, the coulombic efficiency keeps steadily with an average value of 99%. It is found that there is a slight increase in the first several cycles in the case of TiO2/GNRs electrode, which is due to the increase of electrochemical activation [56]. The outstanding electrochemical performances of TiO2/GNRs composite can be associated with the synergistic effects of TiO2 and GNRs....

Show abstract

Synthesis of oxy-hydroxyfluorinated anatase nanoparticles grown on carbon nanotubes

2018, Journal of Fluorine Chemistry

Show abstract

Efficient conductive networks constructed from ultra-low concentration carbon nanotube suspension for Li ion battery cathodes

2018, Carbon

Show abstract

Investigation of counter electrode materials for gel polymer electrolyte based quantum dot sensitized solar cells

2017, Electrochimica Acta

Show abstract

Electrochemical Properties of Transparent Conducting Films of Tantalum-Doped Titanium Dioxide

2017, Electrochimica Acta

Show abstract

Application of Carbon Nanotubes in Lithium-Ion Batteries

2017, Industrial Applications of Carbon Nanotubes

Show abstract

View all citing articles on Scopus

View full text

Copyright © 2010 Elsevier B.V. All rights reserved.

About ScienceDirect Remote access Shopping cart Advertise Contact and support Terms and conditions Privacy policy

Cookies are used by this site. **Cookie settings | Your Privacy Choices**

All content on this site: Copyright © 2024 Elsevier B.V., its licensors, and contributors. All rights are reserved, including those for text and data mining, AI training, and similar technologies. For all open access content, the Creative Commons licensing terms apply.